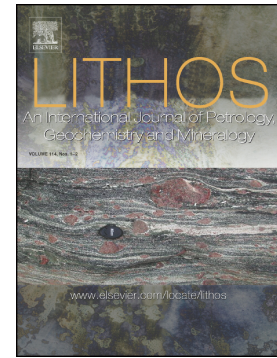


## Journal Pre-proof

Petrogenesis and tectonic implication of the Permian-Triassic syenogranites from the eastern segment of East Kunlun Orogen, China



Vandi Dlama Kamaunji, Lian-Xun Wang, Chang-Qian Ma, Jing Liu, Yu-Xiang Zhu

PII: S0024-4937(20)30567-3

DOI: <https://doi.org/10.1016/j.lithos.2020.105932>

Reference: LITHOS 105932

To appear in: *LITHOS*

Received date: 15 June 2020

Revised date: 4 December 2020

Accepted date: 12 December 2020

Please cite this article as: V.D. Kamaunji, L.-X. Wang, C.-Q. Ma, et al., Petrogenesis and tectonic implication of the Permian-Triassic syenogranites from the eastern segment of East Kunlun Orogen, China, *LITHOS* (2020), <https://doi.org/10.1016/j.lithos.2020.105932>

This is a PDF file of an article that has undergone enhancements after acceptance, such as the addition of a cover page and metadata, and formatting for readability, but it is not yet the definitive version of record. This version will undergo additional copyediting, typesetting and review before it is published in its final form, but we are providing this version to give early visibility of the article. Please note that, during the production process, errors may be discovered which could affect the content, and all legal disclaimers that apply to the journal pertain.

© 2020 Published by Elsevier.

**Petrogenesis and tectonic implication of the Permian-Triassic  
syenogranites from the eastern segment of East Kunlun Orogen, China**

Vandi Dlama **Kamaunji**<sup>a</sup>, Lian-Xun **Wang**<sup>a\*</sup>, Chang-Qian **Ma**<sup>a</sup>, Jing **Liu**<sup>a</sup>, Yu-Xiang **Zhu**<sup>a</sup>

<sup>a</sup>School of Earth Sciences, China University of Geosciences, 430074, Wuhan, P.R. China

\*= Corresponding author. Tel: +86 027-67883139. Fax: +86 027-67883001. Email:  
lianxunwang@cug.edu.cn

Journal Pre-proof

**ABSTRACT**

Permian-Triassic granitoids are widespread in the East Kunlun Orogen (EKO) and are influential in the re-construction of Paleo-Tethyan tectono-magmatic activities. In this contribution, zircon U-Pb dating and Lu-Hf isotopic as well as whole rock major and trace elements analysis have been conducted on a series of syenogranite plutons from the eastern segment of EKO to constrain their petrogenesis and tectonic implication. The syenogranites are characterized by dominant mineral assemblages of K-feldspars and minor plagioclase and biotite, in contrast to the coexisting granodiorites that are rich in amphibole and plagioclase. Zircon U-Pb dating reveals that the studied syenogranites represent a two-stage magmatism from Middle Permian to Late Triassic (ca. 265 Ma and 235–232 Ma). Geochemical and mineralogical evidences show that the syenogranites are classified as high-K calc-alkaline, weakly peraluminous, highly fractionated ( $DI = 93\text{--}95$ ) and moderately fractionated ( $DI = 82\text{--}91$ ) I-type granites. They yield negative  $\epsilon_{\text{Hf}}(t)$  values ( $-13.25$  to  $-0.11$ ), which, together with their high Th/Nb (0.73–4.88), Th/La (0.29–2.65) and La/Nb (1.07–4.48) ratios and moderate pressure conditions (7–10 kbar) imply magma generation through partial melting of the normal-thickened lower crust. The magma underwent extensive plagioclase and subordinate K-feldspar fractionation during evolution. Given the old two-stage Hf model ages ( $T_{\text{DM2}} = 1270\text{--}1100$  Ma), we interpret the ancient lower crust as their dominant source rocks with limited contribution from the juvenile lower crust. Our new data, in tandem with published data show that the Middle-Permian (ca. 265 Ma) Jialuhe syenogranites were formed during a period of local extension concomitant with the northward subduction of the Paleo-Tethyan ocean. In contrast, the Late-Triassic Qingshuihe (235 Ma), Keri (234 Ma), Wutuo (232 Ma) and Balong syenogranite plutons were generated in response to asthenospheric upwelling, lower crust delamination and subsequent continental rifting in a post-collisional extension stage along the convergent plate margins.

**Key words:** East Kunlun Orogen, Syenogranite, Fractionated I-type granite, Permian-Triassic, Paleo-Tethys.

## **Petrogenesis and tectonic implication of the Permian-Triassic syenogranites from the eastern segment of East Kunlun Orogen, China**

Vandi Dlama **Kamaunji**<sup>a</sup>, Lian-Xun **Wang**<sup>a\*</sup>, Chang-Qian **Ma**<sup>a</sup>, Jing **Liu**<sup>a</sup>, Yu-Xiang **Zhu**<sup>a</sup>

<sup>a</sup>School of Earth Sciences, China University of Geosciences, 430074, Wuhan, P.R. China

\*= Corresponding author. Tel: +86 027-67883139. Fax: +86 027-67883001. Email: lianxunwang@cug.edu.cn

### **ABSTRACT**

Permian-Triassic granitoids are widespread in the East Kunlun Orogen (EKO) and are influential in the re-construction of Paleo-Tethyan tectono-magmatic activities. In this contribution, zircon U-Pb dating and Lu-Hf isotopic as well as whole rock major and trace elements analysis have been conducted on a series of syenogranite plutons from the eastern segment of EKO to constrain their petrogenesis and tectonic implication. The syenogranites are characterized by dominant mineral assemblages of K-feldspars and minor plagioclase and biotite, in contrast to the coexisting granodiorites that are rich in amphibole and plagioclase. Zircon U-Pb dating reveals that the studied syenogranites represent a two-stage magmatism from Middle Permian to Late Triassic (ca. 265 Ma and 235–232 Ma). Geochemical and mineralogical evidences show that the syenogranites are classified as high-K calc-alkaline, weakly peraluminous, highly fractionated (DI = 93–95) and moderately fractionated (DI = 82–91) I-type granites. They yield negative  $\epsilon_{\text{Hf}}(t)$  values (–13.25 to –0.11), which, together with their high Th/Nb (0.73–4.88), Th/La (0.29–2.65) and La/Nb (1.07–4.48) ratios and moderate pressure conditions (7–10 kbar) imply magma generation through partial melting of the normal-thickened lower crust. The magma underwent extensive plagioclase and subordinate K-feldspar fractionation during evolution. Given the old two-stage Hf model age ( $T_{\text{DM2}} = 1270\text{--}2100$  Ma), we interpret the ancient lower crust as their dominant source rocks with limited contribution from the juvenile lower crust. Our new data, in tandem with published data show that the Middle-Permian (ca. 265 Ma) Jialuhe syenogranites were formed during a period of local extension concomitant with the northward subduction of the Paleo-Tethyan ocean. In contrast, the Late-Triassic Qingshuihe (235 Ma), Keri (234 Ma), Wutuo (232 Ma) and Balong syenogranite plutons were generated in response to asthenospheric upwelling, lower crust delamination and subsequent continental rifting in a post-collisional extension stage along the convergent plate margins.

**Key words:** East Kunlun Orogen, Syenogranite, Fractionated I-type granite, Permian-Triassic, Paleo-Tethys.

## 1. Introduction

As the most archetypal products of a long-lived orogeny, granitoids are widely studied to reveal the magma generation and differentiation processes that may provide insights into the evolution history of the orogen (e.g., Bellos et al., 2015). The East Kunlun Orogen (EKO) is a key component in the reconstruction of the Proto- and Paleo-Tethys domain along the northern fringes of the Tibetan Plateau (e.g., Li et al., 2018a; b; Yu et al., 2019). The multistage accretion accompanied by arc-continental collision throughout the Early Neoproterozoic to Triassic times triggered the emplacement of voluminous granitoids with abundant mafic microgranular enclaves (MMEs) and minor intermediate to basic intrusions in the East Kunlun Orogen (EKO) (Wu et al., 2020; Xiong et al., 2016; Yu et al., 2019; Zhang et al., 2012; Zhou et al., 2020).

The EKO is renowned for the magma mixing process and crust-mantle interaction, ascribable to the prevalence of MMEs commonly developed in the widespread granodiorites (Chen et al., 2016; Zhang et al., 2012). In comparison, systematic studies on the origin and evolution of the associated syenogranites and their magmatic response to multistage subduction and collisional processes are limited. Several scientific issues related to the syenogranites remain controversial. For example, some studies have shown that the syenogranites in the EKO are predominantly high-K calc-alkaline I-type rocks (e.g., Xiong et al., 2014; 2016; Zhang et al., 2012) whereas others have grouped them into aluminous A-type granites (e.g., Ding et al., 2018; Peng et al., 2016; ). The petrogenetic affinity of the syenogranites and their origin also remain enigmatic (Zhang et al., 2012; Xiong et al., 2014). Whether magma mixing has played a role in the genesis of their parental magmas or they only provide crustal materials for magma mixing to form the granodiorites is unanswered. Further, precisely dating of the syenogranites will

be helpful for the reconstruction of the Paleo-Tethys history, particularly for the timing of the continental collision.

In this contribution, we present detailed zircon U-Pb geochronology, Lu-Hf isotope, and whole-rock major and trace elements data for five representative syenogranite plutons (Qingshuihe, Balong, Keri, Wutuo, and Jialuhe) from the eastern segment of the East Kunlun Orogen (EKO), NW China. We aim to: (1) constrain the magma source and evolution of the syenogranites; (2) shed new lights on the precise timing of the Paleo-Tethyan using the new geochronological data of the syenogranites; (3) investigate the petrogenetic relationship of the syenogranites in relation to the coexisting granodiorites in the East Kunlun Orogen (EKO).

## **2. Regional geologic background**

The Kunlun Orogen extends more than 2500 km in an east-west direction within the northern segment of the Tibetan Plateau and lies wholly within the western part of the Central China Orogenic Belt (Deng et al., 2011) (Fig. 1a). The orogen experienced rapid uplift of the Tibetan Plateau during the recent Cenozoic era and has preserved distinct evidence of the subduction invoked by collision of the three blocks: Tarim, Qaidam and Qiangtang (e.g., Yu et al., 2019). Notably, the strike-slip fault of the Altyn Tagh system divided the Kunlun Orogen into two sub-orogens: East and West Kunlun Orogens (Fig. 1b).

The East Kunlun Orogen (EKO) is bounded by the Qaidam terrane to the north and the Bayan Har terrane to the south (Fig. 1b). It extends >1000 km in an E-W direction and can be further divided into three tectonic units: Northern, Middle and Southern zones, which were separated by the faults of the North and Central Kunlun, respectively (cf.

Jiang et al., 1992). The Southern Kunlun Faults separated the A'nyemaqen–Buqingshan suture zone from the Southern Zone and linked it to the Bayan Har sedimentary Terrane to the south (Fig. 1c). Three magmatic episodes were recognized in the EKO: (1) Neoproterozoic episode, (2) Ordovician-Silurian episode, and (3) Permian-Triassic episodes (e.g., Dong et al., 2018; Yu et al., 2019). The Neoproterozoic episode witnessed the emplacement of coeval S- and A-type granites between 1007–870 Ma, widespread within the Central Kunlun region (e.g., Chen et al., 2015; Dong et al., 2018). The Ordovician-Silurian rocks were emplaced between 495–390 Ma and are mainly A-type with subordinate S- and I-type granitoids (e.g., Chen et al., 2016).

The Permian-Triassic period between 278–200 Ma (e.g., Peng et al., 2016; Xiong et al., 2014; Zhang et al., 2012; Zhou et al., 2020, this study) (Suppl. Table 1) witnessed the largest magmatism in the EKO, during which abundant I-type and restricted A-type granitoids were emplaced within an area of about 25,000 km<sup>2</sup> (e.g., Liu et al., 2004; Dong et al., 2018). These granitic plutons outcropped in an east-west direction, intruding into the stratified Precambrian metamorphic rocks. The granodiorites are the most abundant rock series during the Permian-Triassic period, most of which are coeval with the restricted syenogranites and monzogranites (Suppl. Table 1, Fig. 1c). Plenty of studies have shown that the formation of these granitoids was driven by the northward subduction of the Paleo-Tethys Ocean (e.g., Dong et al., 2018; Xing et al., 2020; Xiong et al., 2014, 2016; Zhang et al., 2012).

The basement of the EKO consist of the Jinshuikou Group that is represented by two Formations: (1) Paleo- to Mesoproterozoic (ca. 1700–1200 Ma) Xiaomiao Formation, characterized by granulite-schist and amphibolites facies as well as metamorphic marbles and quartzites, and (2) Paleoproterozoic (ca. 2200–1800 Ma) Baishahe Formation, which

is composed of abundant gneisses, marbles and amphibolites as well as minor schists and migmatite (Dong et al., 2018; Zhang et al., 2012). The Early Paleozoic (ca. 419–401 Ma) Nachitai Group is a sub-set of the Nuomuhong suture zone and consists of carbonate, metasedimentary, basalts and ultramafic rocks (Wang et al., 2003). The Cambrian to Late Devonian (ca. 516–360 Ma) Buqingshan tectonic mélange zone contains ophiolites, cherts, gabbro as well as limestone and sandstones (cf. Bian et al., 2004), whereas the Bayan Har sedimentary terrane is a Triassic flysch basin containing sandstones and slates (She et al., 2006).

### 3. Local geology and sample description

Five representative syenogranite plutons in the eastern segment of the EKO were investigated, including the Qingshuihe, Balong, Keri, Wutuo and Jialuhe plutons (Fig. 1c & 2a–e). The Qingshuihe pluton is located northwest of Balong County and covers an area of about 20 km<sup>2</sup>. The syenogranites are of restricted occurrences with sharp intrusive contact with the spacious granodiorites (Fig. 2a & 3a). They are typified by pinkish colour with medium-coarse grains of K-feldspars and quartz crystals, in great contrast to the whitish granodiorite with prevalence of amphibole, plagioclase and quartz (Figs. 3a & b). In thin section, the syenogranite is composed of orthoclase (~25%), microcline (~20%), plagioclase (~10%), quartz (~30%), and biotite (~15%) (Fig. 3c).

In the Balong pluton (Fig. 2b), small syenogranite stocks outcropped inside the granodiorite intrusion (Fig. 2b). Most of the syenogranites masses are reddish while the granodiorite country rocks are greyish-white. In hand specimen, tiny specks of dark mafic minerals interlocked within the abundant medium-grained K-feldspars and quartz crystals are discernable (Fig. 3d). Photomicrographs of Balong syenogranites consist of quartz

(35–40%), orthoclase (30–35%), plagioclase (15%) and biotite (10%) (Figs. 3e & f). Accessory phases include magnetite, ilmenite and apatite.

The Keri syenogranite is a small intrusion with an area of about 15km<sup>2</sup> and also intruded into the granodiorite (Fig. 2c). In hand specimen, the dominant leucocratic K-feldspars are recognizable by their light-pinkish and platy characters whereas melanocratic dark mafic minerals are of restricted occurrences (Fig. 3g). Thin section of Keri syenogranites (Figs. 3h) show orthoclase (~35%), plagioclase (~25%), quartz (~20%) and biotite (~15%).

The Wutuo pluton is about 15 km<sup>2</sup> in extent and connected with monzogranite to the north and granodiorite to the south (Fig. 2d). Hand specimen of the syenogranite is medium-coarse grained with crystals of K-feldspars, quartz and minor biotite (Fig. 3i). Thin section of the sample (Figs. 3j) indicates the presence of perthite (~30%), quartz (~25%), plagioclase (~25%), orthoclase (~15%), and biotite (~5%).

The Jialuhe syenogranites are intrusive into the Proterozoic Baishahe Group and the Paleozoic Nachitai Group metamorphic rocks (Figs. 2e & 3k). The outcrop of the Jialuhe syenogranite is about 25 km<sup>2</sup>. The mineral assemblages of Jialuhe syenogranite (Figs. 3l) include quartz (~40%), orthoclase (~35%) and biotite (~15%), with accessory zircon, titanite and magnetite.

## 4. Analytical methods

### 4.1 Whole-rock major and trace element analyses

Major and trace element concentrations were analyzed at the Australian Laboratory Services (ALS) of Guangzhou (China) and the State Key Laboratory of Geological Processing and Mineral Resources (GPMR) in China University of Geosciences, Wuhan respectively. Prior to the analyses, rock samples were pulverized using an agate mill until

the right consistency (< 200 mesh size) is obtained. The major elements compositions were obtained using an ME-XRF 26d spectrometer, with a standard analytical precision of 1 wt.% and detection limit of <0.01 wt.%. The trace element compositions were determined using an Agilent 7700e ICP-MS with analytical precision ranging from 5-10%. Internal standard of AGV-2, BCR-2, RGM-2 and BHVO-2 were adopted in order to monitor any drift which might arise due to mass response. Detailed analytical procedure for sample preparation has been documented by Liu et al. (2008).

### 3.2 LA-ICP-MS zircon U-Pb dating

Zircon grains from five representative samples (17QSH01-1, 17QSH02-1, 17KR03-1, 17WT02-1 and D2037-2) were extracted and the grains were carefully handpicked under a binocular microscope, after which they were fixed onto an epoxy resin, thoroughly polished and coated with a film. The extraction of the cathodoluminescent (CL) images of the zircons was done using a JSMIT100 fixed to a GATAN MINICL device at the Sample Solution Analytical Technology Co., Ltd, Wuhan, China. Zircon U-Pb isotope and trace element concentration were determined using a 193 nm Geo Las Pro and an Agilent 7500a ICP-MS with a laser spot beam of 32  $\mu\text{m}$  at the State Key Laboratory of GPM. For the external standards and calibration of mass discrimination and isotope fractionation, zircon 91500 and zircon GJ-1 were used respectively. A background acquisition time of 18 – 20 seconds and data acquisition time of 50 seconds was adopted for each measurement. The ICP-MS-Data Cal (Excel-base) software (cf. Liu et al., 2008) was used for data processing. More details of analytical procedure and operating conditions could be found in Liu et al. (2010).

### 3.3 Zircon Lu-Hf isotope analyses

In-situ Lu-Hf isotope analysis was conducted at the State Key Laboratory of GPMR, China using a Neptune Plus MC-ICP-MS equipped with a Geolas 193 nm ArF Laser Ablation System (LAS). Measurement was done on the ablation spots close to those for the U-Pb dating with a spot beam of 44  $\mu\text{m}$ . Acquisition of background and ablation signal were done for 20 s and 50 s respectively. The standard ratio of  $^{176}\text{Hf}/^{175}\text{Lu} = 0.02655$  was adopted to correct for atmospheric pressure interference of  $^{175}\text{Lu}$  on  $^{176}\text{Hf}$  while  $^{176}\text{Hf}/^{175}\text{Lu} = 0.5886$  was used for  $^{176}\text{Yb}$  on  $^{176}\text{Hf}$  based on Machado and Simonetti (2001) recommendation. Analytical signal selection and integration as well as mass bias calibration were done using ICP-MS-Data Cal software (cf. Liu et al., 2010). For the epsilon  $\epsilon_{\text{Hf}}(t)$  determination, chondrite ratio of  $^{176}\text{Hf}/^{177}\text{Hf} = 0.282772$  and  $^{176}\text{Lu}/^{177}\text{Hf} = 0.0332$  (after Belousova et al., 2006) was used. The single-stage Hf model ages ( $T_{\text{DM1}}$ ) computations has was done using the depleted mantle ratios ( $^{176}\text{Hf}/^{177}\text{Hf} = 0.28325$  and  $^{176}\text{Lu}/^{177}\text{Hf} = 0.0384$ ) as described by Griffin et al. (2002). The calculations for the crustal Hf model ages ( $T_{\text{DM2}}$ ) was done using  $^{176}\text{Lu}/^{177}\text{Hf} = 0.015$  (after Belousova et al., 2006) as the mean value for the continental crust.

## 5. Analytical results

### 5.1 Whole-rock major element compositions

Whole-rock compositions of 25 studied syenogranites and 452 compiled granitoids from the East Kunlun Orogen (EKO) (contemporaneous intrusions consist of 181 syenogranites, 196 granodiorites and 75 monzogranites) are presented in Table 1 and suppl. Table 2. All the studied syenogranites are highly silicic ( $\text{SiO}_2 = 69.25\text{--}76.93$  wt.%), similar to the compiled syenogranites (average of 74.12 wt.%), but higher than the

compiled granodiorites (average of 66.21 wt.%) (Fig. 4a). The studied syenogranites are generally depleted in  $\text{TiO}_2$  (0.03–0.31 wt.%) and  $\text{MgO}$  (0.07–0.75 wt.%), with low  $\text{Al}_2\text{O}_3$  contents (12.11–16.95 wt.%). They display higher total alkalis ( $\text{Na}_2\text{O}+\text{K}_2\text{O} = 7.21\text{--}10.89$  wt.%, average = 8.21 wt.%) relative to the compiled granodiorites (average of 6.50 wt.%).

They all plot in the sub-alkaline granite field on the Total Alkali-Silica (TAS) diagram (Fig. 4a; after Middlemost, 1994) and predominantly within the syenogranite field on the  $R_1$ - $R_2$  diagram (Fig. 4b; after De la Roche et al., 1980). Similar to majority of the compiled syenogranites and monzogranites, the studied samples are weakly peraluminous ( $\text{ASI} = 1.02\text{--}1.11$ ; Fig. 4c; after Frost et al., 2001) and are plotted strictly within the high-K calc-alkaline field in the chemical discrimination diagram (Fig. 4d; after Peccerillo and Taylor, 1976). The studied syenogranites display higher  $\text{FeO}^{\text{total}} / (\text{FeO}^{\text{total}} + \text{MgO})$  ratios than most of the compiled granodiorites and straddle close to the boundary between the ferroan and magnesian granitoid fields (Fig. 4e; after Frost et al., 2001). They show apparent higher  $\text{Na}_2\text{O}+\text{K}_2\text{O}-\text{CaO}$  contents, obviously in line with the compiled syenogranites and monzogranites, but different from the granodiorites (Fig. 4f; after Frost et al., 2001). Notably, the studied syenogranites show an A-, I- and S-type overlap on Figs. 4g & f. Likewise, on the classical granite discrimination diagrams of Whalen et al. (1987), most of the studied syenogranites are plotted in the I- & S-type fractionated and unfractionated fields except for the Jialuhe syenogranites which are in some cases plotted in the A-type field (Fig. 5). Of note, a large percentage of the compiled syenogranites also plot in the I- & S-type fractionated and unfractionated field, at odd to most of the compiled granodiorites (Fig. 5).

## 5.2 Whole-rock trace element compositions

The primitive mantle normalized diagram of Sun and McDonough, (1989) indicates enrichment of LILE (e.g. Rb, Pb and K), with strong negative Ti, P, Sr and Ba anomalies for all the studied syenogranites, indistinguishable from all the reported syenogranites (Figs. 6a & c). Notably, the trace and REE patterns of studied syenogranites as well as all the compiled syenogranites are reminiscent with the reference lines of lower continental crust of Rudnick and Gao (2003) (Figs. 6a–d).

The rock chondrite-normalized bulk rock diagram shows enrichment in LREE with high normalized ratios [ $(La/Yb)_N = 3.55–22.28$ ] and [ $(La/Sm)_N = 2.12–6.05$ ], a fairly flat HREE signature ( $(Gd/Yb)_N = 0.87–1.85$ ) and significant negative Eu anomalies ( $Eu/Eu^* = 0.11–0.88$ ) for all the studied syenogranites (Fig. 6b; Table 1). Notably, the studied syenogranites display REE patterns similar to the compiled syenogranites and monzogranites (Figs. 6c–h). The granodiorites display weaker negative Eu anomalies compared to other granitoids, probably indicative of less plagioclase fractionation.

The studied syenogranites show variable HFSEs (Nb = 9.4–19.49 ppm; Ta = 0.9–2.93 ppm; Zr = 69.3–273.67; Hf = 2.2–7.85; Sn = 1.19–4.23 ppm; Th = 6.9–47.39 ppm) and LILEs (e.g., Ba = 34–1162 ppm; Rb = 22–265 ppm; Sr = 30–247 ppm; Cs = 0.18–9.39) contents with higher LREE contents (47–298 ppm), relative to the indistinguishable MREE (6.80–21.98 ppm) and HREE (6.48–21.80 ppm) contents. Most of these trace element contents contrast with those of the compiled granodiorites, but closely matches the compiled syenogranites (See Table 1 & Suppl. Table 2).

### 5.3 Zircon U-Pb ages

Analytical results obtained from the LA-ICP-MS zircon U-Pb dating are presented in Table 2. Most of the grains are euhedral to subhedral, ranging in size from 80 to 250  $\mu\text{m}$ . They are characterized by oscillatory magmatic zoning (Fig. 7a-e).

Fifteen zircon grains of Qingshuihe north (17QSH01) and thirteen grains of Qingshuihe south (17QSH02) yield low Th/U ratios (0.20–0.96 and 0.34–0.92, Table 2), diagnostic of magmatic origin (e.g., Belousova et al., 2006). The concordant crystals of Qingshuihe north syenogranite yield  $^{206}\text{Pb}/^{238}\text{U}$  concordia age of  $235.3 \pm 0.6$  Ma (MSWD = 1.60) (Fig. 8a). This matches, within error range the  $^{206}\text{Pb}/^{238}\text{U}$  concordia age of Qingshuihe south syenogranite ( $234.6 \pm 0.6$  Ma, MSWD = 0.28) (Fig. 8b).

Fourteen zircon crystals of Keri syenogranite (17KR03-1) yield  $^{206}\text{Pb}/^{238}\text{U}$  concordia age of  $234.5 \pm 0.5$  Ma (MSWD = 0.002) (Fig. 8c) with low Th/U ratios (0.29–0.67). This is younger than the reported age of granodiorites in the area (ca. 249 Ma, e.g., Xiong et al., 2014).

Twelve analyzed zircon spots of Wutuo syenogranite (17WT03-1) yield  $^{206}\text{Pb}/^{238}\text{U}$  concordia age of  $232.2 \pm 0.7$  Ma (MSWD = 0.89) (Fig. 8d), with low Th/U ratios (0.31 – 0.84). This is relatively younger than the published U-Pb ages of syenogranite (ca. 248–245 Ma, e.g., Li et al., 2018b) and granodiorite in the area (ca. 241 Ma, e.g., Xiong et al., 2014).

Compared to the syenogranites from other studied plutons, the Jialuhe syenogranite (17D237-2), with low Th/U ratio (0.32–0.98) yield relatively higher  $^{206}\text{Pb}/^{238}\text{U}$  concordia age of  $264.9 \pm 1.1$  Ma with MSWD of 0.74 (Fig. 8e) based on twelve analyzed zircon spots. This is much older than the reported U-Pb age of syenogranites in the area (ca. 241–239 Ma, e.g., Liu et al., 2004).

Zircon chondrite diagram of all studied syenogranites display pronounced positive and negative Ce and Eu anomalies respectively, with marked enrichment in HREE and MREE relative to the LREE, consistent with classical magmatic zircons (Fig. 8f).

#### 5.4 Zircon Lu-Hf isotope

Zircon Lu-Hf isotopic compositions of representative syenogranites are presented in Table 3. Fifteen zircon grains of Qingshuihe north syenogranite (17QSH01-1) yield  $^{176}\text{Hf}/^{177}\text{Hf}$  ratios varying from 0.28231 to 0.28258. They show significant negative  $\epsilon\text{Hf}_{(234\text{ Ma})}$  ( $-11.94$  to  $-1.84$ , average =  $-5.48$ ), with Mesoproterozoic to Paleoproterozoic crustal Model ages ( $T_{\text{DM2}} = 2020$  to  $1380$  Ma).

Fourteen analyzed zircon spots of Qingshuihe south syenogranite (17QSH02-1) yield  $^{176}\text{Hf}/^{177}\text{Hf}$  ratios ranging from 0.28239 to 0.28263. The grains yield  $\epsilon\text{Hf}_{(234\text{ Ma})}$  ranging from  $-8.85$  to  $-0.11$  (average =  $-2.52$ ), which corresponds to Mesoproterozoic to Paleoproterozoic crustal Model ages ( $T_{\text{DM2}}$ ) between 1830 to 1270 Ma.

Fourteen zircon grains of Keri syenogranite (17KR03-1) produced  $^{176}\text{Hf}/^{177}\text{Hf}$  ratios of 0.28251 to 0.28258 with less negative  $\epsilon\text{Hf}_{(234\text{ Ma})}$  ( $-4.57$  to  $-1.81$ , average =  $-3.78$ ) and Mesoproterozoic crustal Model ages ( $T_{\text{DM2}} = 1560$  to  $1380$  Ma).

Fifteen zircon grains extracted from Wutuo syenogranite (17WT02-1) show  $^{176}\text{Hf}/^{177}\text{Hf}$  ratios ranging from 0.28226 to 0.28251, corresponding to a wide range of negative  $\epsilon\text{Hf}_{(232\text{ Ma})}$  values ( $-13.25$  to  $-4.11$ , average =  $-6.91$ ). Their Model ages ( $T_{\text{DM2}} = 1530$  to  $2100$  Ma) are typical of Mesoproterozoic to Paleoproterozoic crust.

The fifteen analyzed zircon grains of Jialuhe syenogranite (17D237-2) display  $^{176}\text{Hf}/^{177}\text{Hf}$  ratios from 0.28233 to 0.28243) and yield significant negative  $\epsilon\text{Hf}_{(264\text{ Ma})}$  ( $-10.09$  to  $-6.81$ , average being  $-8.35$ ), depicting Paleoproterozoic crustal model ages ( $T_{\text{DM2}}$ ) from 1930 to 1730 Ma (Table 3).

## 6. Discussion

### 6.1 Petrogenesis of the Permian-Triassic syenogranites

#### 6.1.1 Highly and moderately fractionated I-type granites

The syenogranites from Wutuo and Balong plutons (Group 1) show high differentiation index ( $DI = 93\text{--}95$ ; average of 94; norm  $Qz+Ab+Or$  based on CIPW calculation results; Janousek et al., 2006), typical of highly fractionated granites (93, Thornton and Tuttle, 1960). However, the syenogranites from Keri, Qingshuihe and Jialuhe plutons (Group 2) have lower DI values (82–91; average of 87) which are higher than the normal granites (80, Thornton and Tuttle, 1960). Likewise, their DI values are higher than the Dayaoshan I-type granites (60–70, in southern China, which has been interpreted as weakly fractionated granites (Farag et al., 2020). Hence, we interpret the Group 2 syenogranites as moderately fractionated granites, an interpretation well supported by their higher proportion of mafic mineral (e.g., biotite), relative to the highly fractionated (Group 1) syenogranites (Fig. 3). The higher  $SiO_2$  and  $K_2O$  contents as well as lower  $MgO$ ,  $Al_2O_3$ ,  $CaO$ ,  $FeO_2$ , and  $Na_2O$  contents of the Group 1 syenogranites (Table 1) mirror a higher degree of differentiation compared to the Group 2 syenogranites. Moreover, the Group 1 syenogranites show low contents of Ba, Sr and Eu, with high Rb, Th, U as well as elevated Rb/Sr and lower K/Rb ratios, suggesting highly fractionated granites (e.g., Chappell, 1999).

The complete absence of Al-rich minerals (e.g., garnet, muscovite, tourmaline and cordierite), as also evidenced by their weakly peraluminous affinity ( $ASI = 1.02\text{--}1.11$ , Table 1), suggest that the studied syenogranites are different from S-type granite (Fig. 4c) (Chappell and White, 1974). This identification is also corroborated by the anti-correlation between  $SiO_2$  and  $P_2O_5$  contents (Fig. 9a). The Group 1 syenogranites display

typical fractionated I-type character on the Zr+Nb+Ce+Y diagrams of Whalen et al. (1987; Figs. 5c & d), in contrast to most of the Group 2 syenogranites (except Jialuhe), which show an unfractionated and/or moderately fractionated affinity. We infer that the Jialuhe syenogranites, regardless of their A-type affinity belong to the moderately fractionated I-type granite series, based on their low DI ratios (88–91, Table 1). Besides, the Jialuhe syenogranites show higher CaO contents (average of 1.28 wt.%) relative to the A-type granites (0.75 wt.%), but closely matches the I-type granites (1.71 wt.%; e.g., Whalen et al., 1987). In addition, their HFSEs contents (average of Zr = 273 ppm; Nb = 18 ppm; Y = 46 ppm) are lower than the A-type granites (averages of Zr = 528 ppm; Nb = 37 ppm, Y = 75 ppm, Whalen et al., 1987). The fact that the syenogranites generally show <1% CIPW normative corundum and diopside, also mirror their I-type imprint (Chappell and White, 1974).

Calculated zircon saturation temperatures ( $T_{Zr}$ ) of the studied syenogranites (709–774°C; average of 767°C, excluding Jialuhe) based on Watson and Harrison (1984) model are lower than the typical A-type granites (839°C, e.g., Kings et al., 1997), but relatively similar to the I-type granites (781°C, e.g., Chappell and White, 1992; King et al., 1997). Also, they fall within the  $T_{Zr}$  range of I-type granites in Donghe, SW China (Zhu et al., 2015) (Fig. 9b). However, the calculated  $T_{Zr}$  of the Jialuhe syenogranites (832–836°C, average of 834°C, except for one sample with 787°C) bear resemblance to A-type granites (839°C, e.g., King et al., 1997).

### 6.1.2 Magma source

The studied syenogranites of the eastern segment of the EKO show lower average Mg# (22.51) as well as lower contents of Ni (1.24 ppm), Cr (21.72 ppm), V (8.72 ppm) and Co (1.48 ppm) relative to the mantle-derived granite (Mg# = 60; Ni = 81 ppm; Cr =

151 ppm; V = 151 ppm; Co = 34 ppm; Wu et al., 2020), and mixed source (Mg# = 48; Ni = 42 ppm; Co = 94 ppm; V = 119 ppm; Zhou et al., 2020). However, their low Mg#, Ni, Cr, V and Co contents are similar to the syenogranites reported in the EKO (e.g., Qimantage area, Chen et al., 2001; Elashan Mountain, Wu et al., 2020, Suppl. Table 1), which were interpreted as derivatives of the lower crust. Moreover, the studied syenogranites plot strictly within the pure crustal melt and normal arc fields, contrary to the granodiorites, majority of which plot within the adakite melt fields (Figs. 9c & d). Some trace element ratios (e.g., Th/Nb, Th/La, La/Nb and Nb/Ta) remain constant even during magma differentiation, thus, are being interpreted as reflective of the source nature from which the granites evolved (Shellnutt et al., 2009). The trace element ratios of the studied syenogranites (averages of Th/Nb = 1.60; Th/La = 0.70; La/Nb = 2.61; Nb/Ta = 11.82), are higher than the ratios of primitive mantle (Th/Nb = 0.18; Th/La = 0.13; La/Nb = 0.94; Nb/Ta = 16.00), but closely matches the average ratios of the crust (Th/Nb = 0.44; Th/La = 0.20; La/Nb = 2.2; Nb/Ta = 11–12) (e.g., Weaver, 1991; Green, 1995).

Isotopically, the variably low negative  $\epsilon_{\text{Hf}}(t)$  values ( $-13.25$  to  $-0.11$ , average,  $= -5.45$ ) and two-stage Hf model ages ( $T_{\text{DM}2} = 1270\text{--}2100$  Ma, Table 3) of the studied syenogranites are reflective of source rocks associated with the anatexis of Paleo- and Mesoproterozoic lower crust. Similarly, their  $^{176}\text{Hf}/^{177}\text{Hf}$  ratios (0.28225–0.28262, Table 3) are lower than the average chondritic and depleted ratio ( $\geq 0.28277$ ), but consistent with the lower crust (Fig. 9e) (e.g., Wu et al., 2007). From Middle to Late Triassic, both juvenile and ancient basement crust were present within the lower continental crustal domain underneath the EKO (Xiong et al., 2016; Zhou et al., 2020), either of which is most likely the source for the studied syenogranite plutons. The old Hf model ( $T_{\text{DM}2}$ ) ages of the studied syenogranites (1270–2100 Ma) mirror an ancient lower crust for their

source rocks. This is more plausible as the average  $T_{DM2}$  (ca. 1600 Ma) is much older than the basement in the EKO (Fig. 9f). However, 11 out of the 73 analyzed zircon grains (15%) of the studied syenogranites yield younger Hf model ( $T_{DM2}$ ) ages of 1270–1390 Ma (average of 1340 Ma, Table 3), which probably reflect a contribution of the juvenile crust for the source rock.

Indeed,  $\epsilon_{Hf}(t)$  compositions of zircon crystals that crystallized from a mixed source often show wide range of variation (up to about 10 units, e.g., Davidson et al., 2007). This is exemplified by the relatively wide range of  $\epsilon_{Hf}(t)$  values (–0.10 to –20.10), recently reported for the mixed mantle- and crustal-derived MME-bearing granodiorites in Nangou pluton, EKO (e.g., Yan et al., 2020). In the case of the studied syenogranites, their wide range of  $\epsilon_{Hf}(t)$  values (–13.25 to –20.10, Fig. 10) is probably attributable to the inhomogeneity of the lower crust (e.g., Levanter et al., 1994), rather than mixed source associated with MMEs, because MMEs are rarely observed in the syenogranites. In contrast, MMEs are abundant in the widespread granodiorites as well as restricted monzogranites and monzodiorites plutons in the EKO (Wu et al., 2020; Xiong et al., 2014; Zhou et al., 2020) and their origin has been linked to magma mixing (e.g., Zhou et al., 2020).

### 6.1.3 Partial melting conditions of magma source

The studied syenogranites were juxtaposed with the experimentally-derived cotectic liquids on the pseudo-ternary F–An–Or diagram of Castro (2013), (Fig. 11), an experiment conducted under water-undersaturated conditions ( $\leq 5$  wt.%  $H_2O$ ). The syenogranites aligned well with the cotectic trends of low water (2.30–2.50 wt.%) and moderate pressure (0.7–1.0 GPa; 7.0–10Kbar) conditions, consistent with Heri and Sierra

Nevada batholiths ( $\text{SiO}_2$ : 63–70 wt.%; 2.30 wt.% and 7.0 Kbar) (Fig. 11), believed to have been generated in an oceanic subduction zone (e.g., Sisson et al., 2005). The inferred moderate pressure closely matches the low- $\text{Al}_2\text{O}_3$  (<15 wt.%) pressure of partial melt (< 16 kbar, e.g., Rapp et al., 1991). Moreover, the  $\text{H}_2\text{O}$  contents of the studied syenogranites, extrapolated from the pseudo-ternary diagram agree well with the average  $\text{H}_2\text{O}$  content (2.30 wt.%) of the recently reported Dayaoshan I-type granites in southern China (cf. Dang et al., 2020).

The moderate pressure setting of the studied syenogranites most likely suggests magma generation from the lower crust typified by normal crustal thickness (cf. Xiong et al., 2016). Using the common temperature gradient (about 25°C per km, e.g., Xiong et al., 2016), the temperature is not expected to exceed 750°C. This is much lower compared to the saturation temperature of apatite in the studied syenogranites (765–910°C, Table 1) calculated based on Watson and Harrison (1984) model. Therefore, additional heat source is needed, in line with the high temperature of the studied syenogranites (average of 770 °C) which slightly exceed 750°C. This conforms to the aforementioned inference, i.e., the parental magmas were generated via partial fusion of the lower crust with normal crustal thickness and high thermal gradient (probably >35 °C/km, e.g., Xiong et al., 2016) under prevailing conditions of low pressure and high temperature.

#### *6.1.4 Fractional crystallization*

Fractional crystallization during magma evolution is attested by the marked depletions with respect to Ba, Nb, Sr, P, Ti and Eu on the trace and REE normalized spider diagrams (Figs. 6a & b). Negative Nb-Ti anomalies mirror fractionation of titanium-bearing phases such as ilmenite or titanite, while negative P anomalies is consistent with apatite fractionation, as also evidence by the negative relationship with

$P_2O_5$  and  $SiO_2$  (Fig. 9a). Significant depletion of Eu entails fractionation of plagioclase. Fractionation of K-feldspar would invariably effectuate negative Ba anomalies, while that of plagioclase would initiate negative Sr-Eu anomalies.

The Harker variation diagrams show a marked negative and positive relationships between major elements and  $SiO_2$  contents as well between LILEs and their ratio, whose variations are, to a great extent, controlled by feldspars and biotite (Fig. 12). Plagioclase fractionation is demonstrated by the negative correlation between  $SiO_2$  and  $Al_2O_3$  (Fig. 12a). Marked increase in crystallization increases the  $SiO_2$  contents in the magma. As plagioclase enters the liquidus, the magma is depleted in  $Al_2O_3$  and plagioclase crystallization leads to a decrease in the amount of CaO. These scenarios obviously explain the pronounced negative Eu anomalies (Fig. 6b) because  $Ca^{2+}$  is substituted by  $Eu^{2+}$  in plagioclase (Vasyukova and Williams-Jones, 2019). Decrease in  $Al_2O_3$  as a function of plagioclase separation has been proven experimentally (e.g., Villiger et al., 2007). Extensive plagioclase separation during magmatic evolution is further attested by the correlation between Eu and Sr (Fig. 12b).

Fractionation trends of plagioclase and K-feldspar are displayed on Figs. 12c & d. The compiled granodiorites are clustered towards the end of the evolution trend, with decreasing Rb/Sr ratios from ~0.50 to ~0.05, relative to the syenogranites (~0.50 to ~10.00) (Fig. 12c). This probably implies extensive fractionation of plagioclase by the syenogranite magmas relative to that of the granodiorites. Similarly, the studied syenogranites aligned well with the plagioclase evolution trend much earlier (around 100 ppm), followed by a sharp break (around 300 ppm), typified by K-feldspar and plagioclase fractionation trend (Fig. 12d), indicative of extensive fractionation of

plagioclase and subordinate K-feldspar. The anti-correlations between  $\text{SiO}_2$  with  $\text{TFe}_2\text{O}_3$  and  $\text{TiO}_2$  contents indicate fractionation of magnetite and titanite (Figs. 12e & f).

## 6.2 Geodynamic implications

The EKO has preserved abundant geological records of orogenic subduction and collision events among the three major Block in the region (i.e., Tarim, Qaidam, and Qiangtang) during the Paleo-Tethys Ocean evolution (Roger et al., 2003). Similar to most other orogenic belts, post-collision uplift entails the lithospheric isostatic adjustment when a large load is removed either through lower (thickened) crustal delamination or slab breakoff (Davies and Blanckenburg, 1995), allowing the extensive granitic magmas to be emplaced within the upper crustal level.

The U-Pb zircon age–frequency histograms of the studied syenogranite plutons and the compiled granitoids show that the Late Triassic period recorded the largest magmatism in the EKO whereas the Middle-Permian witnessed a less magmatic flare-up event (Figs. 13a–d, Suppl. Table 1). Hence, it is most likely that the EKO developed into post-collision environment in the Late Triassic period (cf. Dong et al., 2018; Zhou et al., 2020).

The low Sr/Y (0.95–13.96) and La/Yb (5.32–33.43) ratios, as well as high Th/Yb ratios (3.29–21.44) and elevated Yb and Y contents (e.g., Martin, 1999), together with the pronounced Nb and Ta anomalies (Fig. 6a) of the studied Middle-Permian (Ca. 265 Ma) and Late-Triassic (ca. 235–232 Ma) syenogranites from the eastern segment of the EKO demonstrate their ubiquitous “arc signature” (cf. Goss and Kay, 2009). Figs. 14a–d shows a complex tectonic affiliation where all the studied syenogranites including the compiled granitoids straddle the volcanic-arc granite and collisional granite fields, probably representing subduction and post-collision-related granites (Fig. 13a-d).

### 6.2.1 A local extension setting for the Middle-Permian (ca. 265 Ma) syenogranites

The U-Pb zircon age of Jialuhe syenogranite (ca. 265 Ma) overlaps with massive subduction-related granitic magmatism, causing the complexity of their tectonic setting in the EKO. For example, the Early Permian (Ar-Ar age, ca. 278 Ma) Xiaomiao mafic dykes in the EKO were emplaced in a subduction environment (cf. Li et al., 2014), and has been widely accepted as the initial stage of the Paleo-Tethyan northward subduction along the proto-A'nyemaqen suture zone in the east Kunlun orogen (Liu et al., 2014; Peng et al., 2016). Similarly, The Aikedesite subduction-related monzonitic granites in southern EKO yielded a Middle-Permian (ca. 269 Ma, Yang et al., 2013) crystallization age, implying that the southern segment of the EKO was probably the subduction site at this time. Further, the Wulonggou I-type granodiorites emplaced during the Late Permian (ca. 258–260 Ma) display typical continental arc imprints, indicative of subduction-induced magmatism (Li et al., 2014; Luo et al., 2015). These references indicate that the EKO was most likely within a subduction site during Early Permian. This inference could be further evidenced by the A'nyemaqen ophiolite suite, which is overlying unconformably the Late Permian Gequ Formation (Fig. 15a) and consists of deltaic-epieiric carbonate facies including basal conglomerates, calcareous mudstone and sandstone (Wang et al., 2003).

Indeed, initial subduction stage is unlikely to be related to large-scale extension events, because such possibility invariably contradicts the typical formation environment of A-type granites. However, Middle-Late Permian syenogranite has been reported in Dalijigetang complex (ca. 259 Ma; noted as A-type granite) which has been interpreted as an extension product during the episodically northward subduction of the Paleo-Tethyan ocean (Peng et al., 2016). Likewise, local extension during subduction has also been

reported for the Wulonggou Late Permian (ca. 260 Ma) granitoids in the EKO (Luo et al., 2015). As a result, we suggest that the Middle-Late Permian syenogranite observed in Jialuhe intrusion of this work might record some local extension environment during subduction-dominated stage (Fig. 15b).

### 6.2.2 *A post-collisional extension setting for the Late Triassic (ca. 235–232 Ma) syenogranites*

The East Kunlun–Qaidam Terrane and Bayan Har Terrane collided during the Triassic period (Fig. 15c) and consequently formed the FKCP and Buqingshan tectonic mélangé belt (e.g., Li et al., 2018a). This was followed by post-collisional delamination (separation) of the denser lithosphere from the lighter lower crust, consisting of basement materials in both thickened and normal crust (Fig. 15c). The delamination occurred as a result of the marked increase in the density of the lower crust which led to its gravitational instability (Zhang et al., 2007; Magni et al., 2013). The hot upwelling asthenospheric materials occupied the void space created by the delamination and further intensified the delamination, providing heat for the large-scale partial melting of the lower crust (Fig. 15c; Zheng and Chen, 2017). As the continental crust becomes extensively thinned in the Late-Triassic (ca. 235–232 Ma), active continental rifts were generated in which uplift and magmatism as well as metamorphism occurred more extensively due to local buoyancy forces and continuous heating by the upwelling asthenospheric materials (Fig. 15c; cf. Zheng and Zhao, 2017; Zheng and Chen, 2017). This extensive magmatism gave rise to formation of the studied Late-Triassic Qingshuihe (ca. 235 Ma), Keri (ca. 234 Ma), Wutuo (ca. 232 Ma) and Balong syenogranite plutons in a post-collisional extension setting.

As earlier mentioned, the syenogranites generated in the normal ancient lower crust lacked MMEs (Xiong et al., 2014, this study), unlike the granodiorites which formed in the thickened lower crust with predominance of MMEs, ascribable to mixing between crustal and mafic magmas. Hence, their temporal and spatial coexistence in the studied plutons, in part, due to the non-uniform crustal thickness and varied chemical characteristics (e.g., Sr/Y) probably implies that the felsic magmas from ancient lower crust parenting the syenogranites may have provided the crustal magmas for magma mixing to form the MME-bearing granodiorites.

Notably, the formation ages of the studied syenogranites from the eastern segment of the EKO (ca. 265 Ma and ca. 235–232) mark an important evolution that signifies a transition from a local extension setting during the early-stage Paleo-Tethys episodic subduction to the late-stage post-collision (ca. 235–232 Ma), typified by delamination-induced and active rift-related extensive extension tectonic regime.

## 7. Conclusion

1. The syenogranites from the eastern segment of the East Kunlun Orogen (EKO) are high-K calc-alkaline, weakly peraluminous ( $ASI = 1.02\text{--}1.11$ ), moderately fractionated ( $DI = 82\text{--}91$ ) and highly fractionated ( $DI = 93\text{--}95$ ) arc-related I-type granitoids. Combine lines of chemical (e.g., low Mg#, Ni, Cr, V, Co, Th/Nb, Th/La and Nb/Ta contents) and isotopic evidences (e.g.,  $\epsilon_{Hf}(t) = -13.25$  to  $-0.11$ ,  $T_{DM2} = 1270\text{--}2100$  Ma), as well as moderate pressure conditions (7–10 kbar) imply magma generation through partial melting of the Paleo- and Mesoproterozoic normal-thickened lower crust with minor mantle involvement, attributable to the juvenile

lower crust. The magmas underwent extensive fractional crystallization of plagioclase and subordinate K-feldspars and biotite as well as accessory phases.

2. Our present findings, in conjunction with previous literatures indicate that the Middle Permian Jialuhe syenogranites (ca. 265) were formed in a local extension environment during episodic northward subduction of the Paleo-Tethys Ocean.
3. With progressive thinning of the crust during the Late Triassic after delamination and asthenospheric upwelling, active rifts were generated in which extensive magmatic flare ups formed the Qingshuihe (ca. 235 Ma), Keri (ca. 234 Ma), Wutuo (ca. 232 Ma) and Balong syenogranite plutons in a post-collision extension setting.

### **Acknowledgement**

This study was financed by the National Nature Science Foundation of China (No. 42072082, 41530211) and Natural Resource Research Project of Hubei (ZRZY2020KJ04). The two anonymous reviewers as well as the Chief Editor are deeply acknowledged for the constructive and thorough reviews, which greatly improved the paper. Also, the China Scholarship Council (CSC) is deeply appreciated for granting scholarship (20190037) for the first author.

## REFERENCES

- Bellos, L. I., Castro, A., Díaz-Alvarado, J., et al., 2015. Multi-Pulse Cotectic Evolution and In-Situ Fractionation of Calc-Alkaline Tonalite-granodiorite Rocks, Sierra de Velasco Batholith, Famatinian Belt, Argentina. *Gondwana Res.* 27(1): 258–280.
- Belousova, E.A., Griffin, W.L., O'Reilly, S.Y., 2006. Zircon crystal morphology, trace element signatures and Hf isotope composition as a tool for petrogenetic modelling: examples from Eastern Australian granitoids. *J. Petrol.* 47, 329–353.
- Bian, Q.T., Li, D.H., Pospelov, I., Yin, L.M., Li, H.S., Zhao, D.S., Chang, C.F., Luo, X. Q., Gao, S.L., Astrakhansev, O., Chamov, N., 2004. Age, geochemistry and tectonic setting of Buqingshan ophiolites, North Qinghai-Tibet Plateau, China. *J. Asian Earth Sci.* 23, 577–96.
- Castillo, P.R., 2008. Origin of the adakitic high-Nb basalt association and its implications for postsubduction magmatism in Baja California, Mexico. *Geol. Soc. Am. Bull.* 120, 451–462.
- Castro, A., 2013. Tonalite-granodiorite suites as cotectic systems: a review of experimental studies with applications to granitoid petrogenesis. *Earth Sci. Rev.* 124, 68–95.
- Chappell, B.W., 1999. Aluminum saturation in I- and S-type granites and the characterization of fractionated haplogranites. *Lithos* 46, 535–551.
- Chappell, B.W., White, A.J.R., 1974. Two contrasting granite types. *Pacific Geology* 8, 173–174.
- Chappell, B.W., White, A.J.R., 1992. I- and S-type granites in the Lachlan Fold Belt. *Trans. R. Soc. Edinb. Earth Sci.*, 83, 1–26.

- Chen, D.L., Liu, L., Che, Z.C., Luo, J.H., Zhang, Y.X., 2001. Determination and preliminary study of Indosinian aluminous A-type granites in the Qimantag area, southeastern Xinjiang. *Geochimica* 30 (6), 540–546.
- Chen, G., Pei, X.Z., Li, Z.C., Li, R.B., Chen, Y.X., Liu, C.J., Chen, G.C., Wang, X.B., Sang, J.Z., Yang, S., Deng, W.B., 2016. Zircon U-Pb geochronology, geochemical characteristics and geological significance of Chaohuolutaolegai granodiorite in Balong area, East Kunlun Mountains. *Geol. Bull. China* 35(12):1990–2005
- Chen, Y.X., Pei, X.Z., Li, Z.C., Li, R.B., Liu, C.J., Chen, G.C., Pei, L., Wei, B., 2015. Geochronology, geochemical features and geological significance of the granitic gneiss in Balong area, East Section of East Kunlun. *Acta Petrol. Sin.* 31, 2230–2244 (in Chinese with English abstract)
- Dang, Y., Chen, M., Mao, J., Fu, B., 2010. Weakly fractionated I-type granitoids and their relationship to tungsten mineralization: A case study from the early Paleozoic Shangmushui deposit, Dayohe area, South China. *Ore Geol. Rev.* 117, 103281.
- Davidson, J.P., Morgan, D.J., Charlier, B.L.A., Harlou, R., Hora, J.M., 2007. Microsampling and isotopic analysis of igneous rocks: Implications for the study of magmatic systems. *Annu. Rev. Earth Planet. Sci.* 35, 273–311.
- Davies, J.H., Blanckenburg, F.V., 1995. Slab breakoff: a model of lithosphere detachment and its test in the magmatism and deformation of collisional orogens. *Earth Planet. Sci. Lett.* 129, 85–102.
- De la Roche, H., Leterrier, J., Grandclaude, P., Marchal, M., 1980. A classification of volcanic and plutonic rocks using R1R2-diagram and major-element analyses—Its relationships with current nomenclature. *Chem. Geol.* 29, 183-210.

- Deng, W.B., Pei, X.Z., Liu, C.J., Li, Z.C., Li, R.B., Chen, Y.X., Chen, G.C., Yang, S., Chen, G., Sang, J.Z., Wang, X.B. 2016. LA-ICP-MS zircon U-Pb dating of the Chahantaolegai syenogranites in Xiangride area of East Kunlun and its geological significance. *Geol. Bull. China* 35(5), 687–699.
- Ding, Q.F., Song, K., Zhang, Q., Yan, W., Liu, F., 2018. Zircon U–Pb geochronology and Hf isotopic constraints on the petrogenesis of the Late Silurian Shidonggou granite from the Wulonggou area in the Eastern Kunlun Orogen, Northwest China. *Int. Geol. Rev.* 1–24.
- Dong, Y.P., He, D.F., Sun, S.S., Liu, X.M., Zhou, X.M., Zhang, F.F., Zhao, Y., Bin, C., Zhao, G.C., Li, J.H., 2018. Subduction and accretionary tectonics of the East Kunlun orogen, western segment of the Central China Orogenic System. *Earth Sci. Rev.* 186, 231–261.
- Dong, Y.P., Zhang, G.W., Neubauer, F., Liu, X.M., Genser, J., Hauzenberger, C., 2011. Tectonic evolution of the Qinling orogen, China: review and synthesis. *J. Asian Earth Sci.* 41, 213–237.
- Frost, B.R., Arculus, R.J., Barnes, C.G., Collins, W.J., Ellis, D.J., Frost, C.D., 2001. A Geochemical Classification of Granitic Rocks. *J. Petrol.* 42, 2033–2048.
- Green, T.H., 1995. Significance of Nb/Ta as an indicator of geochemical processes in the crust-mantle system. *Chem. Geol.* 120(3–4), 347–359.
- Griffin, W.L., Wang, X., Jackson, S.E., Pearson, N.J., O'Reilly, S.Y., Xu, X., Zhou, X., 2002. Zircon chemistry and magma mixing, SE China: in-situ analysis of Hf isotopes, Tonglu and Pingtan igneous complexes. *Lithos* 61, 237–269.

- Goss, A.R., Kay, S.M., 2009. Extreme high field strength element (HFSE) depletion and near-chondritic Nb/Ta ratios in Central Andean adakite-like lavas (~28°S, ~68°W). *Earth Planet. Sci. Lett.* 279(1–2), 97–109.
- Irvine, T.N., Baragar, W.R.A., 1971. A guide to the chemical classification of the common volcanic rocks. *Can. J. Earth Sci.* 8, 523–548.
- Janousek, V., Farrow, C.M., Erban, V., 2006. Interpretation of whole-rock geochemical data in igneous geochemistry: introducing Geochemical Data Toolkit (GCDkit). *J. Petrol.* 47, 1,255–1,259.
- Jiang, C.F., Yang, J.S., Feng, B.G., Zhu, Z.Z., Zhao, M., Chai, Y.C., Shi, X.D., Wang, H.D., Hu, J.Q., 1992. *Opening-Closing Tectonics of Kunlun Mountains*. Geological Publishing House, 224 pp (In Chinese).
- King, P.L., White, A.J.R., Chappell, B.W., Allen, C.M., 1997. Characterization and origin of aluminous A-type granites from the Lachland fold belt, southeastern Australia. *J. Petrol.* 38, 371–381.
- Levander, A., Hobbs, R. W., Smith, S. K., England, R. W., Snyder, D. B., Holliger, K., 1994. The crust as a heterogeneous “optical” medium, or “crocodiles in the mist”. *Tectonophysics*, 232(1-4), 281-297.
- Li, R.B., Pei, X.Z., Pei, L., Li, Z., Chen, G., Chen, Y., Liu, C., Wang, M., 2018a. The Early Triassic Andean-type Halagatu granitoids pluton in the East Kunlun orogen, northern Tibet Plateau: Response to the northward subduction of the Paleo-Tethys Ocean. *Gondwana Res.* 62, 212–226.
- Li, R.B., Pei, X.Z., Li, Z.C., Pei, L., Chen, G.C., Chen, Y.X., Liu, C.J., Wang, S.M., 2018b. Paleo-Tethys Ocean subduction in eastern section of East Kunlun Orogen:

- Evidence from the geochronology and geochemistry of the Wutuo pluton. *Acta Petrol. Sin.* 34(11), 3399-3421.
- Li, X.H., Li, W.X., Li, Z.H., 2007. On the genetic classification and tectonic implications of the Early Yanshanian granitoids in the Nanling Range, South China. *Chin. Sci. Bull.* 52 (14): 1873–1885.
- Li, X., Yuan, W.M., Hao, N.N., Duan, H.W., Chen, X.N., Mo, X.X., Zhang, A.K., 2014. Characteristics and tectonic setting of granite in Wulonggou area, East Kunlun Mountains. *Global Geology* 33(2), 275–288 (in Chinese with English abstract).
- Liu, B., Ma, C.Q., Zhang, J.Y., Xiong, F.H., Huang, J., and Jiang, H.A., 2014.  $^{40}\text{Ar}$ - $^{39}\text{Ar}$  age and geochemistry of subduction related mafic dikes in northern Tibet, China: petrogenesis and tectonic implications. *Int. Geol. Rev.* 56: 57–73.
- Liu, C.D., Mo, X.X., Luo, Z.H., Yu, X.H., Chen, H.W., Li, S.W., Zhao, X., 2003. Pb-Sr-Nd-O Isotope Characteristics of Granitoids in East Kunlun Orogenic Belt. *Acta Geosci. Sin.* 24, 584–588(in Chinese with English abstract).
- Liu, C.D., Mo, X.X., Luo, Z.H., Yu, X.H., Chen, H.W., Li, S.W., Zhao, X. 2004. Mixing events between the crust- and mantle-derived magmas in Eastern Kunlun: evidence from zircon CHIMP II chronology. *Chinese Sci. Bull.* 49, 828–834.
- Liu, J.N., Feng, C.Y., Qi, F., Li, G.C., Ma, S.C., Xiao, Y., 2012. SIMS zircon U-Pb dating and fluid inclusion studies of Xiadeboli Cu-Mo ore district in Dulan County, Qinghai Province, China. *Acta Petrol. Sin.* 28, 679–690 (in Chinese with English abstract).
- Liu, Y.S., Hu, Z.C., Gao, S., Günther, D., Xu, J., Gao, C.G., Chen, H.H., 2008. In situ analysis of major and trace elements of anhydrous minerals by LA-ICP-MS without applying an internal standard. *Chem. Geol.* 257, 34–43.

- Liu, Y.S., Gao, S., Hu, Z.C., Gao, C.G., Zong, K.Q., Wang, D.B., 2010. Continental and oceanic crust recycling-induced melt-peridotite interactions in the Trans-North China Orogen: U-Pb dating, Hf isotopes and trace elements in zircons of mantle xenoliths. *J. Petrol.* 51, 537–571.
- Luo, M., Mo, X., Yu, X., Li, X., Huang, X., 2015. Zircon U-Pb geochronology, petrogenesis and implication of the Late Permian granodiorite from the Wulonggou area in East Kunlun, Qinghai Province. *Earth Sci. Front.* 22(5), 182–195.
- Machado, N., Simonetti, A., 2001. U–Pb dating and Hf isotopic composition of zircon by laser ablation MC-ICP-MS. In: Sylvester, P. (Ed ), Principles and Applications of Laser-Ablation ICP-Mass Spectrometry in the Earth Sciences. Mineral. Assoc. Canada Short Course 29, 121–144.
- Martin, H., 1999. Adakitic magmas: modern analogues of Archaean granitoids. *Lithos*, 46(3), 411–429.
- Middlemost, E.A.K., 1994. Naming materials in the magma/igneous rock system. *Earth Sci. Rev.* 37, 215–224.
- Patiño Douce, A.E., Johnston, A.D., 1991. Phase equilibria and melt productivity in the pelitic system: implications for the origin of peraluminous granitoids and aluminous granulites. *Contrib. Mineral. Petrol.* 107, 202–218.
- Pearce, J.A., Harris, N., Tindle, A.G., 1984. Trace Element Discrimination Diagrams for the Tectonic Interpretation of Granitic Rocks. *J. Petrol.* 25, 956–983.
- Peccerillo, A. & Taylor, S.R. 1976. Geochemistry of Eocene calc-alkaline volcanic rocks from the Kastamonu area, northern Turkey. *Contrib. Mineral. Petrol.* 58, 63–81.

- Peng, B., Li, B., Zhao, T., Wang, C., Chang, J., Wang, G., Yang, W., 2016. Identification of A-type granite in the southeastern Kunlun Orogen, Qinghai Province, China: implications for the tectonic framework of the Eastern Kunlun Orogen. *Geol. J.* 52(3), 454–469.
- Rapp, R.P., Watson, E.B., Miller, C.F., 1991. Partial melting of amphibolite/eclogite and the origin of Archean trondhjemites and tonalites. *Precambrian Res.* 51, 1–25.
- Rapp, R.P., Watson, E.B., 1995. Dehydration melting of metabasalt at 8–32 kbar: implications for continental growth and crust–mantle recycling. *J. Petrol.* 36, 891–931.
- Roger, F., Arnaud, N., Gilder, S., Tapponnier, P., Jolivet, M., Brunel, M., Malavieille, J., Xu, Z., Yang, J., 2003. Geochronological and geochemical constraints on Mesozoic suturing in east central Tibet. *Tectonics* 22 (4), 1037.
- Roger, F., Jolivet, M., Malavieille, J., 2000. Tectonic evolution of the Triassic fold belts of Tibet. *C. R. Geosci.* 340, 131–9.
- Rudnick, R.L., Gao, S., 2003. Composition of the continental crust. *Treatise Geochem.* 1–64.
- She, Z., Ma, C., Mosen, R., Li, J., Wang, G., Lei, Y., 2006. Provenance of the Triassic Songpan-Ganzi flysch, west China. *Chem. Geol.* 231, 159–75.
- Shellnutt, G.J., Wang, C.Y., Zhou, M.F., Yang, Y., 2009. Zircon Lu–Hf isotopic compositions of metaluminous and peralkaline A-type granitic plutons of the Emeishan large igneous province (SW China): Constraints on the mantle source. *J. Asian Earth Sci.* 35(1), 45–55.
- Sisson, T., Ratajeski, K., Hankins, W., Glazner, A., 2005. Voluminous granitic magmas from common basaltic sources. *Contrib. Mineral. Petrol.* 148, 635–661.

- Sun, S.S., McDonough, W.F., 1989. Chemical and Isotopic Systematics of Oceanic Basalts: Implications for Mantle Composition and Processes. In: Saunders, A.D. and Norry, M.J., Eds., *Magmatism in the Ocean Basins* 42, Geol. Soc. Spec. Publ. 42(1) 313–345.
- Taylor, S.R., McLennan, S.M., 1985. *The Continental Crust: Its Composition and Evolution*. Oxford Press, Blackwell, 1–312.
- Thornton, C.P., Tuttle, O.F., 1960. Chemistry of igneous rocks – Part 1, differentiation index. *Am. J. Sci.* 258 (9), 664–684.
- Vasyukova, O. and Williams-Jones, A., 2019. Partial melting, fractional crystallisation, liquid immiscibility and hydrothermal mobilisation – A ‘recipe’ for the formation of economic A-type granite-hosted HFSE deposits, *Lithos* 356–357, 105300.
- Villiger, S., Müntener, O., Ulmer, P., 2007. Crystallization pressures of mid-ocean ridge basalts derived from major element variations of glasses from equilibrium and fractional crystallization experiments. *J. Geophys. Res. Solid Earth*, 112(B1).
- Wang, G.C., Jia, C.X., Zhu, Y.H. 2003. Regional geological report of Alake Lake Map. China University of Geosciences Press, 165 pp (in Chinese).
- Watson, E.B., Harrison, T.M., 1984. The behavior of apatite during crustal anatexis: Equilibrium and kinetic considerations. *Geochim. Cosmochim. Acta.* 48(7), 1467–1477.
- Weaver, B.L. 1991. The origin of ocean island basalt end member compositions: trace element and isotopic constrains. *Earth Planet. Sci. Lett.* 104(2-4), 381–397.
- Whalen, J.B., Currie, K.L., Chappell, B.W., 1987. A-type granites; Geochemical Characteristics, Discrimination and Petrogenesis. *Contrib. Mineral. Petrol.* 95(4), 407-419.

- Wu, D.Q., Sun, F.Y., Pan, Z.C., Tian, N., 2020. Geochronology, geochemistry, and Hf isotopic compositions of Triassic igneous rocks in the easternmost segment of the East Kunlun Orogenic Belt, NW China: implications for magmatism and tectonic evolution, *Int. Geol. Rev.* 1–21
- Wu, F.Y., Li, X.H., Zheng, Y.F., Gao, S., 2007. Lu–Hf isotopic systematics and their applications in petrology. *Acta Petrol. Sin.* 23(2), 185–220 (in Chinese with English abstract).
- Xing, H.Q., Li, X.W., Xu, J.F., Mo, X.X., Shan, W., Yu, H.X., Hu, J.Q., Huang, X.F., Dong, G.C., 2020. The genesis of felsic magmatism during the closure of the Northeastern Paleo-Tethys Ocean: Evidence from the Heri batholith in West Qinling, China. *Gondwana Res.* 84, 38–51.
- Xiong, F.H., Ma, C.Q., Zhang, J.Y., Jau, B., 2012. The origin of mafic microgranular enclaves and their host granodiorites from East Kunlun, northern Qinghai-Tibet Plateau: implications for magma mixing during subduction of Paleo-Tethyan lithosphere. *Mineral. Petrol.* 104, 211–224.
- Xiong, F., H., Ma, C.Q., Zhang, G., Liu, B., Jiang, H., 2014. Reworking of old continental lithosphere: an important crustal evolution mechanism in orogenic belts, as evidenced by Triassic I-type granitoids in the East Kunlun orogen, Northern Tibetan Plateau. *J. Geol. Soc. London*, 171, 847–863.
- Xiong, F.H., Ma, C.Q., Jiang, H.A., Zhang, H., 2016. Geochronology and Petrogenesis of Triassic High-K Calc-Alkaline Granodiorites in the East Kunlun Orogen, West China: Juvenile Lower Crustal Melting during Post-Collisional Extension. *J. Earth Sci.* 27(3), 474–490.

- Xu, Y.G., Yang, Q.J., Lan, J.B., Luo, Z.Y., Huang, X.L., Shi, Y.R., Xie, L.W., 2012. Temporal–spatial distribution and tectonic implications of the batholiths in the Gaoligong-Tengliang-Yingjiang area, western Yunnan: constraints from zircon U–Pb ages and Hf isotopes. *J. Asian Earth Sci.* 53, 151–175.
- Yan, J., Sun, F., Qian, Y., Tian, N., Yan, Z., Zhang, Y., Yang, X., 2020. Petrogenesis and tectonic implications of the Late Triassic Nangou granodiorite porphyry in the Eastern Kunlun Orogenic Belt, northern Tibetan Plateau. *Can. J. Earth Sci.* 1–13.
- Yang, Y.Q., Li, B.Y., Xu, Q.L., Zhang, B.S., 2013. Zircon U–Pb ages and its geological significance of the monzonitic granite in the Ahegdelesite, Eastern Kunlun, Northwest. *Geol.* 46, 56–62 (in Chinese with English abstract).
- Yin, H.F., Zhang, K.X., Chen, N.S., 2003. 1:25000 Regional Geological Survey Report of Donggeicuona Zone. Wuhan: China University of Geosciences Press.
- Yu, M., Dick, J. M., Feng, C., Li, B., & Wang, H., 2019. The tectonic evolution of the East Kunlun Orogen, northern Tibetan Plateau: a critical review with an integrated geodynamic model. *J. Asian Earth Sci.* 104168.
- Zen, E.A., 1986. Aluminum Enrichment in Silicate Melts by Fractional Crystallization: Some Mineralogic and Petrographic Constraints. *J. Petrol.* 27(5), 1095–1117.
- Zhang, J.Y., Ma, C.Q., Xiong, F.H., Liu, B., 2012. Petrogenesis and tectonic significance of the Late Permian–Middle Triassic calc-alkaline granites in the Balong region, eastern Kunlun Orogen, China. *Geol. Mag.* 149(5), 892–908.
- Zheng, Y.F., Chen, R.X., 2017. Regional metamorphism at extreme conditions: Implications for orogeny at convergent plate margins. *J. Asian Earth Sci.* 145, 46–73.

Zheng, Y.F., Zhao, Z.F., 2017. Introduction to the structures and processes of subduction zones. *J. Asian Earth Sci.* 145, 1–15.

Zhou, H., Zhang, D., Wei, J., Wang, D., Santosh, M., Shi, W., Chen, J., Zhao, X., 2020. Petrogenesis of Late Triassic mafic enclaves and host granodiorite in the Eastern Kunlun Orogenic Belt, China: Implications for the reworking of juvenile crust by delamination-induced asthenosphere upwelling. *Gondwana Res.* 84, 52–70.

Zhu, R.Z., Lai, S.C., Qin, J.F., Zhao, S.W., 2015. Early-Cretaceous highly fractionated I-type granites from the northern Tengchong block, western Yunnan, SW China: Petrogenesis and tectonic implications. *J. Asian Earth Sci.* 100, 145–163.

### Figure Caption

**Fig. 1.** (a) Tectonic framework of the Central China Orogen (modified from Dong et al., 2011); (b) Tectonic outline of the Tibetan Plateau showing the location of the East Kunlun Orogen (EKO) (modified from Roger et al. 2008), (c) Simplified geological map showing the distribution of granitoids in the East Kunlun Orogen (EKO) (after Yin et al. 2003), (d) Geological map of the eastern segment of the EKO showing the studied syenogranite plutons (Modified from 1:250,000 Donggeicuona geological map sheet). QDB-Qaidam Block; EKO- East Kunlun Orogen; COB; Kunlun Orogenic Belt; NCC-North China Craton; SCB-South China Block; TRMB-Tarim Block; ALTF- Altyn Tagh Fault. <sup>(1)</sup> Liu et al. (2004), <sup>(2)</sup> Zhang et al. (2012), <sup>(3)</sup> Deng et al. (2016), <sup>(4)</sup> Xiong et al.

(2014), <sup>(5)</sup> Xiong et al. (2012), <sup>(6)</sup> Yang et al. (2013), <sup>(7)</sup> Liu et al. (2012), <sup>(8)</sup> Xiong et al. (2016), <sup>(9)</sup> Wu et al. (2020). All ages are in million years (Ma).

**Fig. 2.** Geological map of the studied plutons **(a)** Qingshuihe north and south (Exacted from 1:250,000 Donggeicuona geological map sheet), **(b)** Balong (modified from Zhang et al., 2012), **(c)** Keri (Exacted from 1:250,000 Donggeicuona geological map sheet), **(d)** Wutuo (Modified from Yin et al., 2003), **(e)** Jialuhe (Exacted from 1:250,000 Donggeicuona geological map sheet). 1-Quaternary; 2-Late Triassic Elashan Formation; 3-Early Paleozoic Nacitai Group; 4-Mesoproterozoic Xiaomiac Formation; 5-granodiorite; 6-porphyrific-like monzogranites; 7-syenogranite; 8-ultramafic-mafic rocks; 9-angular unconformity; 10-mylonitization/fault.

**Fig. 3.** Hand specimen and petrographic study of syenogranites from the eastern segment of EKOB **(a)** sharp intrusive contact between granodiorite and syenogranites in Qingshuihe pluton with visible mesocratic and leucocratic mineral assemblages of varying grained sizes, **(b)** Qingshuihe south syenogranite hand specimen sample with visible K-feldspars, quartz and minor dark minerals, **(c)** Photomicrograph of Qingshuihe south syenogranites showing the presence of quartz (Qtz), orthoclase (Orth), biotite (Bt), plagioclase (Pl) and microcline (Mcl), **(d)** Hand specimen sample of Balong syenogranite with leucocratic K-feldspars and quartz, and minor specks of mesocratic mafic minerals, **(e-f)** Photomicrographs of Balong syenogranites with mineral assemblages of quartz (Qtz), biotite (Bt), orthoclase (Orth) and plagioclase (Pl), **(g)** Hand specimen sample of Keri syenogranite with clear quartz and K-feldspar crystals, **(h)** Photomicrograph of Keri syenogranite typified by mineral assemblages of quartz (Qtz), orthoclase (Orth), biotite (Bt) and plagioclase (Pl), **(i)** Hand specimen of Wutuo syenogranites characterized by

coarse-grained crystals of K-feldspars, quartz and restricted dark mafic minerals, **(j)** Photomicrographs of Wutuo syenogranites showing quartz (Qtz), orthoclase (Orth), biotite (Bt), plagioclase (Pl) and perthite (Perth), **(k)** sharp intrusive contact between the Jialuhe medium-coarse syenogranites and the metamorphic rocks of the Nachitai Group, **(l)** Photomicrographs of Jialuhe syenogranites showing the presence of quartz (Qtz), orthoclase (Orth) and biotite (Bt). All photomicrographs of rock samples are viewed under cross-polarized light (XPL).

**Fig. 4.** Chemical classification and nomenclature of the syenogranites from the eastern segment of EKOB: **(a)** Silica versus Total Alkali Silica (TAS) diagram (after Middlemost, 1994). The dashed line represents the division between Alkaline and Cal-alkaline fields (after Irvine and Baragar, 1971), **(b)**  $R_1$ - $R_2$  diagram (after De la Roche et al., 1980), **(c)** ASI versus A/NK diagram (after Frost et al., 2001). The dashed line dividing the peraluminous domain into weakly and strongly fields is as summarized by Zen (1986), **(d)**  $\text{SiO}_2$  versus  $\text{K}_2\text{O}$  diagram (after Peccerillo and Taylor, 1976), **(e)**  $\text{SiO}_2$  versus  $\text{FeOt}/(\text{FeOt}+\text{MgO})$  (after Frost et al., 2001), **(f)**  $\text{SiO}_2$  versus  $(\text{Na}_2\text{O} + \text{K}_2\text{O} - \text{CaO})$  (after Frost et al., 2001). Correlation data of published granitoids are presented in Supplementary Table 2.

**Fig. 5 (a–d)** Chemical discrimination diagrams (after Whalen et al., 1987). Correlation data of published granitoids are presented in Supplementary Table 2.

**Fig. 6 (a)** Primitive-mantle-normalized trace element spider diagram of studied syenogranites from the eastern segment of EKOB, **(b)** chondrite-normalized REE distribution of the studied syenogranites, **(c & d)** Primitive-mantle and chondrite normalized diagrams of published granitoids in the East Kunlun Orogen (EKO).

Normalized values for the primitive-mantle and chondrite REE diagrams were taken from Sun and McDonough (1989) and Taylor and McLennan (1985) respectively. Data of published granitoids are presented in Supplementary Table 2.

**Fig. 7 (a-e)** cathodoluminescent (CL) images of representative zircon crystals the studied syenogranites analyzed for U-Pb and Lu-Hf isotopes. Samples: **(a)** 17QSH01-1 (Qingshuihe north pluton), **(b)** 17QSH02-1 (Qingshuihe south pluton), **(c)** 17KR03-1 (Keri pluton), **(d)** 17WT02-1 (Wutuo pluton), **(e)** D2037-2-1 (Jialuhe pluton). Red cycle indicates points of Lu-Hf isotope analyses whereas yellow cycle represents points of U-Pb zircon age analyses.

**Fig. 8 (a-e)** Concordia plots LA-ICP-MS zircon U-Pb ages, **(f)** Normalized zircon chondrite REE distribution of syenogranites from the eastern segment of the EKO. Normalization standards for the zircon REE diagram were from Taylor and McLennan (1985).

**Fig. 9.** Plots of **(a)**  $\text{SiO}_2$  versus  $\text{P}_2\text{O}_5$ , **(b)** ASI versus  $T_{\text{Zr}}$  **(c)** Mg# versus  $\text{SiO}_2$  (after Patiño Douce and Johnston, 1991; Rapp and Watson, 1995), **(d)** Y versus Sr/Y (after Castillo, 2008), **(e)** Age versus  $^{176}\text{Hf}/^{177}\text{Hf}$ , **(f)** Age versus  $\varepsilon\text{Hf}$  (t). Zircon saturation temperature was calculated using the method of Watson and Harrison (1984); highly-fractionated I-type granites in Fogang, South China are from Li et al. (2007); while those from Donghe and Chayu, South West China are from Xu et al. (2012) and Zhu et al. (2015), respectively. Whole-rock major and trace element as well as zircon Hf data of published granitoids are presented in Supplementary Table 2 and Supplementary Table 3 respectively.

**Fig. 10** Zircon  $\epsilon_{\text{Hf}}$  (t) distribution of the studied syenogranites and their corresponding histograms.

**Fig. 11.** F(FeO+MgO+MnO)-An-Or diagram summarizing the most relevant cotectic relations of the studied syenogranites at variable pressures and initial water contents. Assimilation (a) and restite-unmixing (ru) vectors are indicated in relation to metasedimentary (greywackes and pelites) sources (after Castro, 2013). Correlation data of Sierra Nevada batholith (California) and Heri Batholith (West Qinling) were gotten from Sisson et al. (2005) and Xing et al. (2020) respectively. Correlation data of the published granitoids are same as in Fig. 9 and are presented in Supplementary Table 2.

**Fig. 12.** Selected major and trace element diagrams of the studied syenogranites showing fractionation trends of major and accessory mineral phases **(a)**  $\text{SiO}_2$  versus  $\text{Al}_2\text{O}_3$ , **(b)** Eu versus Sr, **(c)** Sr versus Rb/Sr, **(d)** Ba versus Sr, **(e & f)**  $\text{SiO}_2$  versus  $\text{TFe}_2\text{O}_3$  and  $\text{TiO}_2$ . Correlation data of published granitoids are presented in Supplementary Table 2.

**Fig. 13.** Histograms of **(a)** U-Pb zircon ages of the studied syenogranites from the eastern segment of EKO, **(b–d)** Concordia/mean U-Pb and SHRIMP ages of the published syenogranites (N = 32), granodiorites (N = 52) and monzogranites (N = 12) in the EKO. Published ages of granitoids are presented in Supplementary Table 1.

**Fig. 14 (a–d)** Granite tectonic discrimination diagrams (after Pearce et al., 1984), Correlation data of published granitoids are presented in Supplementary Table 2.

**Fig. 15 (a)** Stratigraphy of the EKO (modified after Li et al., 2018a), **(b & c)** schematic cartoons showing the multi-stage tectono-magmatic evolution of the syenogranites from the eastern segment the EKO.

Journal Pre-proof

Table 1. Major and trace element compositions of I-type syenogranites of Qingshuihe-Jialuhe region

Samples	Published granitoids in EKO			This study	Qingshuihe north syenogranites				Qingshuihe north syenogranites			D
	Grano	Monzo	Syeno	Syeno	QSH01-1	QSH01-3	QSH01-5	QSH01-6	QSH02-1	QSH02-3	QSH03-1	
SiO <sub>2</sub>	66.21	71.90	74.56	74.12	74.10	72.99	73.45	74.84	70.61	70.00	69.25	
TiO <sub>2</sub>	0.50	0.26	0.17	0.16	0.18	0.15	0.18	0.18	0.31	0.30	0.20	
Al <sub>2</sub> O <sub>3</sub>	15.73	14.27	12.84	13.34	13.42	13.81	13.84	13.42	14.78	14.99	16.95	
Fe <sub>2</sub> O <sub>3</sub>	2.93	1.74	1.30	1.84	1.78	1.47	1.81	1.80	2.69	2.59	1.68	
MnO	0.12	0.05	0.05	0.05	0.06	0.06	0.07	0.07	0.09	0.09	0.06	
MgO	1.59	0.66	0.28	0.30	0.43	0.37	0.44	0.44	0.71	0.75	0.49	
CaO	3.69	1.70	1.02	1.16	0.97	1.08	1.30	1.19	2.34	2.24	2.61	
Na <sub>2</sub> O	3.51	3.57	3.19	3.69	3.78	3.71	3.94	3.81	3.99	3.97	4.72	
K <sub>2</sub> O	2.99	3.94	4.93	4.31	3.88	4.5	3.95	3.97	3.52	3.67	3.70	
P <sub>2</sub> O <sub>5</sub>	0.12	0.09	0.04	0.04	0.06	0.05	0.06	0.04	0.10	0.09	0.06	
LOI				0.81	1.15	0.92	0.80	0.86	0.86	0.72	0.84	
Total				99.78	99.81	99.11	99.84	100.6	100	99.41	100.5	
FeOt	3.10	1.97	1.24	1.66	1.60	1.32	1.63	1.62	2.42	2.33	1.51	
Na <sub>2</sub> O+K <sub>2</sub> O	6.50	7.52	8.13	8.12	7.66	8.21	7.89	7.78	7.51	7.64	8.42	
K <sub>2</sub> O/Na <sub>2</sub> O	0.98	1.15	1.54	1.16	1.03	1.21	1.01	1.04	0.88	0.92	0.78	
Mg#	58.3	46.5	36.85	22.51	32.37	33.27	32.31	32.63	34.34	36.46	36.62	
ASI				1.04	1.10	1.07	1.06	1.06	1.02	1.04	1.03	
A/NK				1.24	1.29	1.26	1.29	1.27	1.42	1.43	1.44	
TZr (°C)				770	740	740	770	741	764	767	709	
Ap.Sat(°C)				826	895	866	889	902	910	894	847	
Q					34.72	31.17	32.15	34.46	28.15	27.21	21.49	
Or					22.97	26.59	23.34	23.46	20.80	21.69	21.87	
Ab					31.51	31.39	33.34	32.24	33.76	33.59	39.94	
DI					20.64	89.46	88.83	90.16	82.71	82.49	83.29	
C					0.96	0.99	0.86	0.79	0.39	0.63	0.58	
Di					0.00	0.00	0.00	0.00	0.00	0.00	0.00	
Li	27.57	99.7	12.27	36.33	27.00	33.20	36.20	35.10	22.60	28.30	21.70	
Be	1.91	7.04	2.53	2.92	2.30	1.80	2.10	1.90	2.20	2.30	2.70	
Sc	8.80	3.9	3.95	4.16	4.70	4.20	4.90	4.60	5.60	5.80	4.10	
V	65.77	22.2	8.86	8.77	11.50	9.50	11.6	12.10	22.30	22.50	13.40	
Cr	18	17.8	12.07	11.72	30.80	24.60	37.8	30.50	39.90	25.90	18.20	
Co	24	28.7	9.61	1.48	1.50	1.50	1.70	1.90	3.30	3.30	2.10	
Ni	20	3.95	13.34	1.24	1.10	1.30	1.70	1.10	1.40	1.10	0.90	
Cu	22.02	14.0	6.77	1.21	0.80	0.60	0.80	0.60	1.10	0.90	1.00	
Zn	57.20	35.0	27.41	33.29	20.9	18.5	21.50	20.50	37.30	38.10	28.00	
Ga	18.37	19.0	18.16	16.68	14.40	13.80	14.80	14.00	15.70	15.60	16.20	
Rb	102.14	109.0	133.56	176.6	142.1	154.2	141.9	141.5	117.3	136.4	117.1	
Sr	339.71	201.0	94.98	115.6	123.2	134.1	141.5	129.1	229.9	222.2	247.1	
Y	16.62	23.4	37.46	27.47	32.90	23.70	30.40	27.50	24.90	26.00	17.70	
Zr	159.31	149.5	195.83	145.05	84.50	88.20	129.6	89.90	134.4	137.1	69.30	
Nb	9.85	99.7	17.90	14.34	15.10	12.40	14.30	13.10	12.30	12.80	9.40	
Sn	-	-	6.19	2.35	2.40	1.90	2.40	2.30	1.80	1.80	1.40	
Cs	4.50	16.12	4.91	4.82	4.00	3.80	4.40	4.00	2.60	2.60	2.30	
Ba	713.18	429.4	399.76	541.82	468.9	605.2	506.1	477.0	418.8	441.7	486.3	
La	30.95	24.7	43.06	37.98	22.10	19.80	24.80	23.70	21.20	19.70	10.1	
Ce	57.44	50.7	83.92	75.43	44.40	39.50	50.00	48.40	43.20	40.60	23.00	
Pr	6.20	5.64	10.28	8.13	4.90	4.40	5.50	5.30	5.00	4.80	3.00	
Nd	22.59	21.9	36.03	28.71	17.50	15.40	19.60	18.70	18.6	17.70	11.8	
Sm	4.13	4.3	6.88	5.56	3.80	3.20	4.10	4.10	4.10	4.00	2.90	
Eu	1.00	0.7	1.75	0.69	0.60	0.60	0.70	0.60	0.9	0.90	0.80	
Gd	3.56	4.3	6.45	4.66	3.80	3.00	3.80	3.70	3.60	3.60	2.70	
Tb	0.54	0.72	0.97	0.79	0.70	0.60	0.70	0.70	0.60	0.60	0.40	
Dy	3.00	4.32	6.23	4.61	4.80	3.60	4.50	4.10	3.90	3.80	2.70	
Ho	0.59	0.86	1.25	0.92	1.00	0.70	1.00	0.90	0.80	0.80	0.60	
Er	1.70	2.79	4.01	2.70	3.20	2.30	2.90	2.60	2.40	2.50	1.60	
Tm	0.26	0.38	0.64	0.41	0.50	0.40	0.50	0.40	0.40	0.40	0.30	

Yb	1.66	2.56	3.74	2.72	3.50	2.60	3.40	2.90	2.70	2.90	1.90
Lu	0.26	0.4	0.57	0.41	0.50	0.40	0.50	0.40	0.40	0.50	0.30
Hf	3.76	4.2	3.66	4.64	3.00	2.90	4.00	3.00	4.0	3.90	2.20
Ta	1.79	1.7	4.96	1.29	1.50	1.10	1.20	1.10	1.10	1.10	0.90
Tl				0.90	0.70	0.80	0.70	0.70	0.60	0.70	0.60
Pb	18.19	22.2	63.48	27.38	21.20	23.90	22.40	21.30	20.6	21.90	24.90
Th	12.96	14.4	26.09	22.25	11.50	10.30	12.60	12.40	13.4	11.40	6.90
U	2.54	3.7	5.56	2.67	1.70	1.30	1.50	1.30	3.30	2.70	1.30
P	541	380	166	153	262.0	218	262	262.0	436.0	393	262.0
K	24828	32712	37346	35805	32210	37357	32791	32957	29221	30466	30716
Ti	2979	1545	1031	975.0	1079	899.0	1079	1079	1858	1798	1199
ΣREE	134	116	209	173	111	96.39	122	116	108	103	62.05
δEu	0.82	0.72	0.65	0.44	0.49	0.60	0.55	0.47	0.72	0.73	0.88
(La/Yb) <sub>N</sub>	15.24	9.31	10.37	10.85	4.53	5.48	5.23	5.90	5.53	4.85	3.83
(Gd/Yb) <sub>N</sub>	1.94	1.45	1.49	1.38	0.87	0.92	0.89	1.02	1.06	0.99	1.13
(La/Sm) <sub>N</sub>	4.76	4.08	4.49	4.15	3.58	3.81	3.72	3.56	3.18	3.03	2.14

Table 1 (Cont.)

Rock types	Wutuo syenogranites				Balong syenogranites						Keri syenogranites		
Samples	WT02-1	WT04-1	WT07-1	WT08-1	XMH01	XMH02	XMH04	XMH06	XMH07	XMH08	KR01-1	KR02-1	KR03-1
SiO <sub>2</sub>	76.13	76.39	75.84	76.52	76.84	76.33	75.66	74.62	75.16	76.79	72.08	76.93	71.23
TiO <sub>2</sub>	0.07	0.06	0.06	0.08	0.13	0.13	0.11	0.18	0.14	0.11	0.26	0.03	0.21
Al <sub>2</sub> O <sub>3</sub>	12.86	12.43	12.67	12.77	12.50	12.56	12.48	12.94	12.88	12.11	14.17	12.39	13.85
Fe <sub>2</sub> O <sub>3</sub> T	1.49	1.38	1.31	1.41	1.16	1.19	1.14	1.55	1.32	1.08	2.62	1.04	2.22
MnO	0.04	0.03	0.03	0.03	0.03	0.02	0.02	0.04	0.03	0.03	0.07	0.02	0.06
MgO	0.09	0.08	0.07	0.09	0.15	0.15	0.11	0.33	0.23	0.12	0.74	0.07	0.59
CaO	0.59	0.59	0.35	0.66	0.56	0.38	0.63	1.24	0.76	0.7	1.95	0.66	1.90
Na <sub>2</sub> O	3.71	3.55	3.55	3.59	3.56	3.47	3.4	3.55	3.53	3.59	3.74	4.25	3.60
K <sub>2</sub> O	4.82	4.67	4.72	4.77	4.73	4.82	5.05	4.49	4.92	4.76	3.63	3.64	3.61
P <sub>2</sub> O <sub>5</sub>	0.01	0.01	0.01	0.01	0.01	0.01	0.01	0.03	0.02	0.0	0.07	0.01	0.08
LOI	0.74	0.63	0.62	0.47	0.57	0.49	0.48	0.56	0.35	0.43	1.01	0.42	2.32
Total	100.55	99.82	99.23	100.4	100.24	99.55	99.09	99.53	99.34	99.55	100.34	99.46	99.64
FeOt	1.34	1.24	1.18	1.27	1.04	1.07	1.03	1.39	1.19	0.97	2.36	0.94	2.00
Na <sub>2</sub> O+K <sub>2</sub> O	8.53	8.22	8.27	8.36	8.29	8.29	8.45	8.04	8.4	8.17	7.37	7.89	7.21
K <sub>2</sub> O/Na <sub>2</sub> O	1.30	1.32	1.33	1.33	1.33	1.39	1.49	1.26	1.39	1.41	0.97	0.86	1.00
Mg#	10.69	10.3	9.57	11.23	20.39	19.98	16.05	22.67	25.66	18.04	35.88	11.77	34.49
ASI	1.04	1.04	1.09	1.04	1.04	1.08	1.02	1.00	1.03	1.01	1.04	1.02	1.05
A/NK	1.14	1.14	1.16	1.15	1.14	1.15	1.15	1.21	1.16	1.13	1.41	1.13	1.41
TZr (°C)	750	764	771	774	764	773	771	765	766	768	775	723	738
Ap.Sat (°C)	769	771	766	772	775	770	774	839	811	775	890	776	850
Q	34.74	36.52	36.31	35.87	36.64	36.75	35.08	34.73	33.89	37.14	31.36	34.80	31.67
Or	28.49	27.60	27.89	28.19	27.95	28.49	29.84	27.54	29.08	28.25	21.45	21.51	21.33
Ab	31.39	30.04	30.04	30.38	30.12	29.36	28.77	31.04	30.87	28.69	31.65	34.96	30.46
DI	94.62	94.16	94.24	94.44	94.72	94.35	93.69	93.30	93.84	94.07	84.46	91.27	83.47
C	0.49	0.49	0.98	0.53	0.57	0.97	0.30	0.06	0.41	0.11	0.71	0.282	0.757
Di	0.00	0.00	0.00	0.00	0.00	0.00	0.00	0.00	0.00	0.00	0.00	0.00	0.00
Li	61.88	43.86	64.48	60.04	49.95	45.04	38.95	32.31	37.56	40.74	28.85	10.3	27.98
Be	4.10	3.89	4.94	4.70	2.70	3.15	2.58	3.62	3.6	2.83	2.83	3.68	3.05
Sc	3.13	3.15	3.13	2.22	2.97	2.90	2.53	3.12	3.32	2.96	4.67	1.13	4.29
V	1.69	2.00	2.43	2.25	3.48	2.73	2.81	9.51	6.84	2.08	24.22	1.35	22.34
Cr	44.22	26.1	34.15	59.32	1.09	1.06	0.91	1.95	2.3	1.04	32.32	14.23	22.81
Co	0.42	0.39	0.66	0.42	0.52	0.63	0.46	1.62	1.28	0.52	4.16	0.57	3.54
Ni	1.09	1.04	1.12	1.11	0.86	0.99	0.92	2.23	1.79	1.03	2.91	0.61	2.27
Cu	0.89	1.21	0.95	0.80	1.73	1.14	1.06	1.49	1.40	0.83	4.41	2.34	1.49
Zn	31.62	44.22	22.53	31.09	17.93	21.35	22.14	23.71	20.92	15.75	51.19	20.65	40.29
Ga	17.7	18.51	18.31	17.93	16.48	15.83	15.92	16.21	16.43	15.54	16.72	15.57	16.29
Rb	250.3	250.0	265.8	260.9	231.7	226.2	220.2	205.6	243.9	237.2	162.2	204.5	139.3
Sr	30.1	32.93	38.98	29.64	77.26	64.65	75.21	128.2	95.96	79.63	185.5	30.15	171.2
Y	28.64	24.6	28.85	31.71	16.93	16.34	14.35	16.5	21.84	18.3	16.36	19.84	18.23
Zr	100.5	117.5	121.8	131.8	114.7	124.4	130.1	128.1	124.1	126.9	143.2	71.27	90.51
Nb	16.29	18.83	16.17	19.49	14.92	11.63	12.33	11.6	13.98	12.36	11.85	9.71	11.88
Sn	4.23	3.46	3.37	4.03	1.19	2.19	1.80	1.72	1.85	1.24	2.86	3.51	2.27

Cs	9.39	6.18	7.74	7.80	5.18	8.46	5.38	5.30	6.41	5.30	7.39	7.87	8.85
Ba	173.8	198.4	217.7	169.6	598.5	637.8	680.8	646.0	518.9	600.5	432.6	34.56	493.7
La	29.32	28.55	26.38	30.47	45.26	45.65	47.13	40.98	36.59	40.81	31.8	17.89	30.96
Ce	65.67	62.55	55.83	67.15	86.91	87.77	90.01	78.67	72.66	78.61	60.61	40.72	56.43
Pr	7.42	7.06	6.6	7.68	9.19	9.1	9.46	7.96	7.81	8.28	6.1	4.73	5.85
Nd	27.23	26.07	23.93	28.45	30.32	30.05	31.16	26.11	26.83	27.15	19.96	16.77	19.78
Sm	6.37	6.00	5.54	6.66	5.1	5.04	5.08	4.17	4.97	4.62	3.5	3.79	3.60
Eu	0.29	0.3	0.32	0.28	0.48	0.52	0.53	0.62	0.46	0.49	0.57	0.12	0.52
Gd	5.09	5.08	4.82	5.47	3.46	3.25	3.27	3.05	4.05	3.13	2.74	3.01	2.91
Tb	0.81	0.8	0.82	0.93	0.63	0.57	0.54	0.5	0.64	0.55	0.45	0.50	0.48
Dy	4.68	4.57	4.61	5.23	3.08	2.82	2.68	2.54	3.70	2.99	2.51	3.04	2.79
Ho	0.88	0.89	0.92	1.01	0.58	0.58	0.49	0.51	0.73	0.61	0.51	0.6	0.56
Er	2.51	2.43	2.66	2.95	1.7	1.58	1.47	1.58	2.18	1.74	1.50	1.83	1.67
Tm	0.37	0.35	0.42	0.42	0.25	0.23	0.21	0.23	0.33	0.27	0.23	0.30	0.26
Yb	2.44	2.39	2.64	2.8	1.61	1.56	1.41	1.58	1.92	1.73	1.62	2.21	1.88
Lu	0.36	0.35	0.38	0.41	0.27	0.23	0.22	0.25	0.31	0.28	0.25	0.35	0.29
Hf	4.01	4.37	4.28	4.94	4.17	4.32	4.41	4.03	4.52	4.44	4.13	3.69	3.02
Ta	1.43	1.37	1.50	1.60	1.42	1.19	1.00	1.39	1.11	1.17	1.35	2.93	1.54
Tl	1.31	1.34	1.28	1.34	1.33	1.21	1.10	0.97	1.08	1.19	0.81	0.92	0.63
Pb	35.09	36.69	34.27	34.82	31	29.87	26.7	21.6	24.86	29.01	27.89	46.24	25.30
Th	25.56	28.65	27.15	38.87	32.46	28.47	29.14	22.21	30.27	20.94	19.51	39.39	18.77
U	2.90	3.60	4.10	4.38	2.77	2.70	2.55	2.84	2.32	1.87	2.46	2.87	3.17
P	43.60	43.60	43.60	43.60	43.60	43.60	43.60	131	87.3	43.6	305	43.6	218
K	40013	38768	39183	39598	39266	40013	41123	37274	40843	39681	30134	30217	29968
Ti	420	360	360	480	779	779	655	1079	839	659	1558	180	1259
ΣREE	132.3	95.9	127.9	153.4	188.8	188.9	193.7	168.7	163.2	171.3	147.4	135.9	159.9
δEu	0.16	0.17	0.19	0.14	0.35	0.40	0.40	0.53	0.32	0.40	0.57	0.11	0.49
(La/Yb) <sub>N</sub>	8.60	8.57	7.17	7.81	20.21	20.91	23.9	18.67	13.69	16.96	14.11	5.81	11.82
(Gd/Yb) <sub>N</sub>	1.66	1.69	1.46	1.56	1.71	1.66	1.85	1.54	1.68	1.44	1.35	1.09	1.23
(La/Sm) <sub>N</sub>	2.83	2.93	2.93	2.81	5.41	5.57	5.71	6.05	4.53	5.43	5.59	2.90	5.29

Grano = Granodiorite, Monzo = Monzogranite, Syc10 = syenogranite. All oxide are in weight percent (wt. %), while trace element are in part per million (ppm).

Differentiation index (DI) = Quartz (Q) + Orthoclase (Or) + Albite (Ab); C (Corundum), Di (Diopside),

Table 2. LA-ICP-MS Zircon U-Pb data for Qingshuihe-Jialuhe syenogranites

Samples/ Spot No.	Element concent. (ppm)		Ratio Th/U	Isotopic Ratios			Isotopic Ages (Maa)					
	Th	U		<sup>207</sup> Pb/ <sup>235</sup> U	1σ	Rho	<sup>207</sup> Pb/ <sup>235</sup> U	<sup>206</sup> Pb/ <sup>238</sup> U	1σ			
Qingshuihe north (17QSH01-1)												
17QSH01-1-4	371	495	0.75	0.2607	0.0084	0.0372	0.0004	0.3432	235	7	235	3
17QSH01-1-1	220	306	0.72	0.2584	0.0124	0.0369	0.0004	0.2276	233	10	233	3
17QSH01-1-2	219	429	0.51	0.2578	0.0098	0.0368	0.0004	0.3000	233	8	233	3
17QSH01-1-7	78	120	0.65	0.2626	0.0153	0.0374	0.0005	0.2345	237	12	237	3
17QSH01-1-8	332	504	0.66	0.2624	0.0087	0.0374	0.0003	0.2483	237	7	237	2
17QSH01-1-9	130	310	0.42	0.2574	0.0097	0.0374	0.0004	0.2554	233	8	236	3
17QSH01-1-10	230	1013	0.23	0.2599	0.0074	0.0371	0.0004	0.3450	235	6	235	2
17QSH01-1-11	112	141	0.79	0.2598	0.0156	0.0374	0.0006	0.2705	234	13	237	4
17QSH01-1-12	305	1502	0.20	0.2551	0.0057	0.0378	0.0003	0.3893	231	5	239	2
17QSH01-1-17	375	1532	0.24	0.2545	0.0054	0.0366	0.0003	0.3834	230	4	232	2
17QSH01-1-3	246	421	0.58	0.2602	0.0079	0.0366	0.0004	0.3569	235	6	232	2
17QSH01-1-14	216	258	0.84	0.2545	0.0094	0.0377	0.0004	0.2789	230	8	239	2
17QSH01-1-15	278	253	0.96	0.2615	0.0098	0.0376	0.0004	0.2944	236	8	238	3
17QSH01-1-18	216	401	0.54	0.2591	0.0087	0.0370	0.0004	0.2924	234	7	234	2
17QSH01-1-20	196	496	0.40	0.2603	0.0087	0.0371	0.0004	0.3462	235	7	235	3
Qingshuihe south syenogranites (17QSH02-1)												
17QSH02-1-1	422	826	0.51	0.2583	0.0074	0.0372	0.0004	0.3417	233	6	236	2
17QSH02-1-3	299	325	0.92	0.2586	0.0114	0.0367	0.0004	0.2266	234	9	232	2
17QSH02-1-4	267	781	0.34	0.2598	0.0083	0.0377	0.0004	0.2926	235	7	238	2
17QSH02-1-7	229	579	0.40	0.2571	0.0083	0.0370	0.0004	0.3083	234	7	234	2
17QSH02-1-10	275	632	0.44	0.2595	0.0071	0.0370	0.0004	0.3508	234	6	234	2
17QSH02-1-12	104	270	0.38	0.2584	0.0118	0.0372	0.0005	0.2964	233	10	236	3
17QSH02-1-13	266	518	0.51	0.2572	0.0078	0.0367	0.0004	0.3341	232	6	232	2
17QSH02-1-14	274	655	0.42	0.2588	0.0085	0.0369	0.0003	0.2813	234	7	234	2
17QSH02-1-17	237	554	0.43	0.2518	0.0081	0.0366	0.0004	0.3723	228	7	232	3
17QSH02-1-18	420	745	0.56	0.2631	0.0072	0.0375	0.0003	0.2814	237	6	237	2
17QSH02-1-19	391	778	0.50	0.2606	0.0054	0.0364	0.0003	0.4323	235	4	231	2
17QSH02-1-20	378	737	0.51	0.2509	0.0073	0.0370	0.0003	0.2962	227	6	234	2
Keri syenogranites (17KR03-1)												
17KR03-1-1	191	386	0.49	0.2608	0.0086	0.0364	0.0003	0.2390	235	7	231	2
17KR03-1-2	271	526	0.51	0.2570	0.0070	0.0367	0.0003	0.3410	232	6	232	2
17KR03-1-3	113	242	0.47	0.2585	0.0098	0.0369	0.0004	0.2643	233	8	233	2
17KR03-1-4	248	369	0.67	0.2609	0.0088	0.0373	0.0003	0.2690	235	7	236	2
17KR03-1-5	249	457	0.55	0.2597	0.0095	0.0376	0.0004	0.2853	234	8	238	2
17KR03-1-7	301	680	0.44	0.2608	0.0068	0.0372	0.0003	0.2750	235	5	235	2
17KR03-1-8	464	1323	0.35	0.2569	0.0054	0.0373	0.0002	0.2937	232	4	236	1
17KR03-1-9	109	303	0.36	0.2557	0.0086	0.0365	0.0003	0.2526	231	7	231	2

17KR03-1-10	373	976	0.38	0.2606	0.0056	0.0372	0.0003	0.3403	235	5	236	2
17KR03-1-11	89.0	280	0.32	0.2555	0.0087	0.0364	0.0003	0.2792	231	7	231	2
17KR03-1-12	207	375	0.55	0.2649	0.0088	0.0372	0.0004	0.2998	239	7	236	2
17KR03-1-14	438	1025	0.43	0.2659	0.0068	0.0371	0.0002	0.2486	239	5	235	1
17KR03-1-17	458	1560	0.29	0.2603	0.0060	0.0370	0.0002	0.2841	235	5	234	2
17KR03-1-18	191	491	0.39	0.2606	0.0079	0.0376	0.0003	0.3033	235	6	238	2
Wutuo syenogranites (17WT02-1)												
17WT02-1-2	77.2	151	0.51	0.2567	0.0156	0.0366	0.0006	0.2839	232	13	232	4
17WT02-1-3	186	328	0.57	0.2575	0.0113	0.0368	0.0005	0.2992	233	9	233	3
17WT02-1-4	134	231	0.58	0.2579	0.0116	0.0369	0.0005	0.3159	233	9	234	3
17WT02-1-7	277	331	0.84	0.2542	0.0119	0.0365	0.0004	0.2498	230	10	231	3
17WT02-1-9	778	1919	0.41	0.2565	0.0051	0.0366	0.0003	0.45.0	232	4	232	2
17WT02-1-10	432	836	0.52	0.2581	0.0069	0.0368	0.0005	0.3535	233	6	233	2
17WT02-1-12	176	559	0.31	0.2565	0.0076	0.0364	0.0003	0.3237	232	6	231	2
17WT02-1-14	199	349	0.57	0.2562	0.0121	0.0364	0.0004	0.2417	232	10	230	3
17WT02-1-16	371	653	0.57	0.2556	0.0089	0.0365	0.0004	0.2858	231	7	231	2
17WT02-1-17	541	699	0.77	0.2583	0.0084	0.0367	0.0004	0.3724	233	7	232	3
17WT02-1-13	728	1528	0.48	0.2543	0.0067	0.0373	0.0004	0.3799	230	5	236	2
17WT02-1-8	1059	2987	0.35	0.2693	0.0053	0.0377	0.0004	0.5344	242	4	232	2
Jialuhe syenogranites (17D20372-1)												
D2037-2-1	543	1422	0.38	0.3136	0.0080	0.0428	0.0006	0.5290	277	6	270	4
D2037-2-3	304	958	0.32	0.3022	0.0085	0.0425	0.0009	0.7661	268	7	268	6
D2037-2-4	225	416	0.54	0.2964	0.0113	0.0417	0.0007	0.4121	264	9	264	4
D2037-2-10	438	860	0.51	0.3122	0.0091	0.0425	0.0007	0.5379	276	7	269	4
D2037-2-11	722	736	0.98	0.3048	0.0098	0.0428	0.0006	0.4196	270	8	270	4
D2037-2-12	223	435	0.51	0.2840	0.0091	0.0401	0.0007	0.5365	254	7	254	4
D2037-2-13	282	648	0.43	0.2961	0.0088	0.0417	0.0006	0.4856	263	7	263	4
D2037-2-15	302	624	0.48	0.2982	0.0096	0.0420	0.0007	0.4891	265	8	265	4
D2037-2-16	492	938	0.52	0.3083	0.0103	0.0432	0.0007	0.4850	273	8	273	4
D2037-2-17	388	547	0.71	0.2914	0.0098	0.0411	0.0005	0.3834	260	8	260	3
D2037-2-18	102	208	0.49	0.2827	0.0159	0.0400	0.0009	0.3797	253	13	253	5
D2037-2-19	307	517	0.59	0.3004	0.0102	0.0422	0.0006	0.4097	267	8	267	4

Table 3. Zircon Lu-Hf isotope compositions of Qingshuihe-Jialuhe syenogranites

Spot no.	Age	$^{176}\text{Yb}/^{177}\text{Hf}$	$^{176}\text{Lu}/^{177}\text{Hf}$	$^{176}\text{Hf}/^{177}\text{Hf}$	$1\sigma$	$\varepsilon\text{Hf} (t)$	$T_{\text{DM}} (\text{Ma})$	$T_{\text{DM2}} (\text{Ma})$	$f_{\text{Lu/Hf}}$
Qingshuihe north syenogranites (17QSH01-1)									
17QSH01-1-01	235	0.042266	0.0017	0.28253	0.000010	-3.39	1030	1480	-0.95
17QSH01-1-02	235	0.054456	0.0022	0.28247	0.000009	-5.5	1130	1610	-0.93
17QSH01-1-03	235	0.045082	0.0018	0.28254	0.000009	-3.1	1020	1460	-0.95
17QSH01-1-04	235	0.060785	0.0024	0.28245	0.000009	-6.32	1170	1670	-0.93
17QSH01-1-05	235	0.050524	0.0020	0.28251	0.000010	-4.06	1060	1520	-0.94
17QSH01-1-06	235	0.072026	0.0028	0.28241	0.000009	-7.71	1230	1750	-0.91
17QSH01-1-07	235	0.031524	0.0013	0.28258	0.000009	-1.84	960	1380	-0.96
17QSH01-1-08	235	0.057240	0.0023	0.28249	0.000009	-4.94	1110	1580	-0.93
17QSH01-1-09	235	0.056667	0.0023	0.28245	0.000011	-6.17	1160	1660	-0.93
17QSH01-1-10	235	0.089623	0.0035	0.28233	0.000009	-10.5	1370	1920	-0.89
17QSH01-1-11	235	0.035162	0.0015	0.28257	0.000009	-2.48	0990	1420	-0.96
17QSH01-1-12	235	0.046303	0.0019	0.28252	0.000009	-3.67	1050	1500	-0.94
17QSH01-1-13	235	0.050119	0.0020	0.28248	0.000009	-5.14	1110	1590	-0.94
17QSH01-1-14	235	0.101718	0.0040	0.28229	0.000009	-11.94	1450	2020	-0.88
17QSH01-1-15	235	0.051453	0.0021	0.28247	0.000008	-5.61	1130	1620	-0.94
Qingshuihe south syenogranites (17QSH02-1)									
17QSH02-1-02	235	0.091143	0.0037	0.28238	0.000011	-8.85	1310	1830	-0.89
17QSH02-1-03	235	0.064001	0.0026	0.28244	0.000008	-6.76	1190	1690	-0.92
17QSH02-1-04	235	0.027863	0.0014	0.28259	0.000009	-1.45	0940	1360	-0.96
17QSH02-1-05	235	0.048165	0.0022	0.28255	0.000009	-2.69	1010	1440	-0.93
17QSH02-1-06	235	0.017327	0.0009	0.28250	0.000011	-4.44	1050	1550	-0.97
17QSH02-1-07	235	0.046736	0.0021	0.28254	0.000008	-3.17	1030	1470	-0.94
17QSH02-1-08	235	0.036847	0.0018	0.28257	0.000008	-1.86	970	1380	-0.94
17QSH02-1-09	235	0.030741	0.0016	0.28261	0.000008	-0.74	920	1310	-0.95
17QSH02-1-10	235	0.034703	0.0017	0.28260	0.000008	-0.94	930	1330	-0.95
17QSH02-1-11	235	0.037802	0.0018	0.28261	0.000008	-0.75	930	1310	-0.94
17QSH02-1-12	235	0.040842	0.0019	0.28260	0.000008	-0.83	930	1320	-0.94
17QSH02-1-13	235	0.048353	0.0021	0.28257	0.000008	-2	980	1390	-0.94
17QSH02-1-14	235	0.037451	0.0017	0.28261	0.000008	-0.62	920	1310	-0.95
17QSH02-1-15	235	0.037367	0.0018	0.28262	0.000009	-0.11	900	1270	-0.95
Keri syenogranites (17KR03-1)									
17KR03-1-01	234	0.0416	0.0012	0.28258	0.000019	-3.54	1030	1490	-0.96
17KR03-1-02	234	0.0484	0.0014	0.28255	0.000021	-3.73	1040	1510	-0.96
17KR03-1-03	234	0.0271	0.0008	0.28254	0.000017	-4.28	1050	1540	-0.98
17KR03-1-04	234	0.0625	0.0018	0.28254	0.000018	-4.53	1080	1560	-0.95
17KR03-1-05	234	0.0230	0.0007	0.28253	0.000018	-1.81	950	1380	-0.98
17KR03-1-06	234	0.0764	0.0021	0.28252	0.000027	-3.96	1060	1520	-0.94
17KR03-1-07	234	0.0366	0.0011	0.28252	0.000015	-2.76	990	1440	-0.97
17KR03-1-08	234	0.0080	0.0004	0.28252	0.000027	-3.21	980	1470	-1.01
17KR03-1-10	234	0.0211	0.0006	0.28251	0.000015	-3.71	1020	1500	-0.98
17KR03-1-11	234	0.0448	0.0013	0.28251	0.000019	-4	1050	1520	-0.96
17KR03-1-12	234	0.0196	0.0006	0.28251	0.000019	-3.08	1000	1460	-0.98
17KR03-1-13	234	0.0629	0.0018	0.28251	0.000020	-4.27	1070	1540	-0.95
17KR03-1-14	234	0.0508	0.0015	0.28250	0.000020	-4.03	1050	1530	-0.95
17KR03-1-15	234	0.0594	0.0017	0.28250	0.000019	-4.57	1080	1560	-0.95
Wutuo syenogranites (17WT02-1)									
17WT02-1-01	232	0.0224	0.0009	0.28246	0.000009	-5.84	1110	1640	-0.97
17WT02-1-02	232	0.0119	0.0005	0.28251	0.000009	-4.26	1040	1540	-0.99
17WT02-1-03	232	0.0172	0.0007	0.28250	0.000008	-4.67	1060	1570	-0.98
17WT02-1-04	232	0.0873	0.0026	0.28225	0.000013	-13.25	1460	2100	-0.92

17WT02-1-05	232	0.0306	0.0012	0.28247	0.000010	-5.75	1110	1630	-0.96
17WT02-1-06	232	0.0383	0.0014	0.28241	0.000008	-7.69	1200	1760	-0.96
17WT02-1-07	232	0.0345	0.0013	0.28244	0.000007	-6.54	1150	1680	-0.96
17WT02-1-08	232	0.0208	0.0008	0.28251	0.000009	-4.11	1040	1530	-0.98
17WT02-1-09	232	0.0415	0.0015	0.28241	0.000008	-7.76	1200	1760	-0.96
17WT02-1-10	232	0.0405	0.0015	0.28242	0.000009	-7.36	1180	1730	-0.96
17WT02-1-11	232	0.0435	0.0015	0.28239	0.000010	-8.37	1220	1800	-0.96
17WT02-1-12	232	0.0267	0.0011	0.28248	0.000010	-5.21	1090	1600	-0.97
17WT02-1-13	232	0.0619	0.0020	0.28236	0.000013	-9.63	1290	1880	-0.94
17WT02-1-14	232	0.0524	0.0019	0.28240	0.000010	-7.93	1220	1770	-0.94
17WT02-1-15	232	0.0224	0.0009	0.28248	0.000010	-5.35	1090	1610	-0.97

## Jialuhe syenogranites (17D2037-02)

D2037-2-01	264	0.1094	0.0029	0.28241	0.000028	-9.77	1350	1910	-0.91
D2037-2-02	264	0.0438	0.0012	0.28240	0.000025	-7.9	1230	1790	-0.96
D2037-2-03	264	0.1221	0.0033	0.28240	0.000030	-9.74	1360	1910	-0.9
D2037-2-04	264	0.0722	0.0020	0.28240	0.000028	-7.57	1230	1770	-0.94
D2037-2-05	264	0.0900	0.0024	0.28239	0.000023	-8.02	1260	1800	-0.93
D2037-2-06	264	0.0716	0.0020	0.28239	0.000037	-7.5	1230	1770	-0.94
D2037-2-07	264	0.0563	0.0015	0.28238	0.000023	-6.5	1260	1830	-0.95
D2037-2-08	264	0.0717	0.0020	0.28238	0.000033	-8.13	1260	1810	-0.94
D2037-2-09	264	0.0765	0.0022	0.28238	0.000044	-6.31	1210	1730	-0.93
D2037-2-10	264	0.0664	0.0018	0.28237	0.000024	-7.68	1230	1780	-0.95
D2037-2-11	264	0.0763	0.0021	0.28236	0.000026	-10.08	1340	1930	-0.94
D2037-2-12	264	0.0638	0.0018	0.28233	0.000020	-10.09	1330	1930	-0.95
D2037-2-13	264	0.0582	0.0015	0.28233	0.000021	-8.74	1270	1850	-0.95
D2037-2-14	264	0.0404	0.0011	0.28232	0.000025	-7.35	1200	1760	-0.97
D2037-2-15	264	0.0531	0.0015	0.28232	0.000026	-7.44	1220	1770	-0.95

**Declaration of interests**

The authors declare that they have no known competing financial interests or personal relationships that could have appeared to influence the work reported in this paper.

Lianxun Wang

On behalf of all co-authors

Journal Pre-proof

## Highlights

1. The syenogranites from eastern EKOB were emplaced at 265 Ma and 235–232 Ma.
2. The syenogranites are highly to moderately fractionated I-type granitoids.
3. The syenogranites were originated from ancient lower crust.
4. They formed in extension settings during episodic subduction and post-collision.

Journal Pre-proof

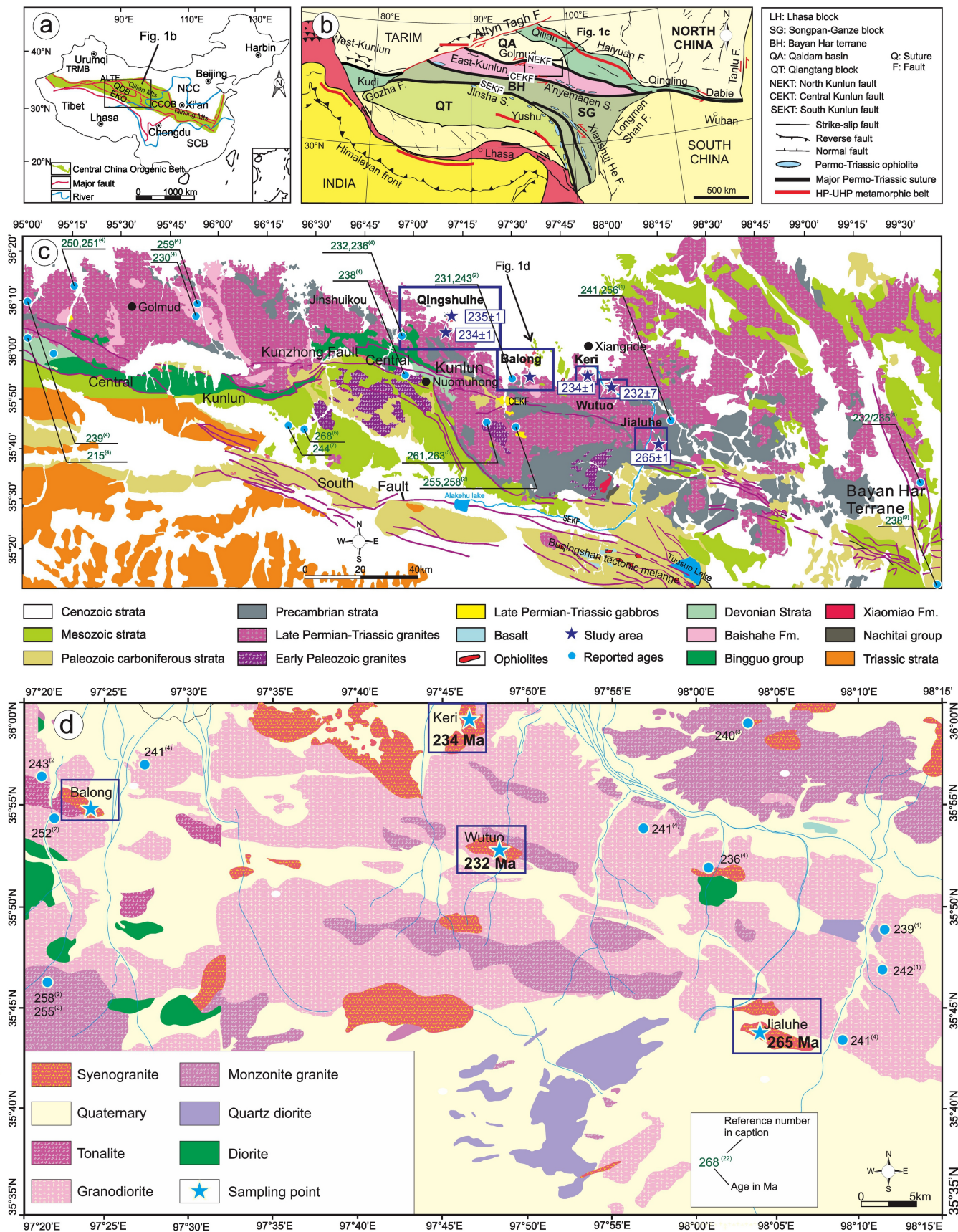


Figure 1

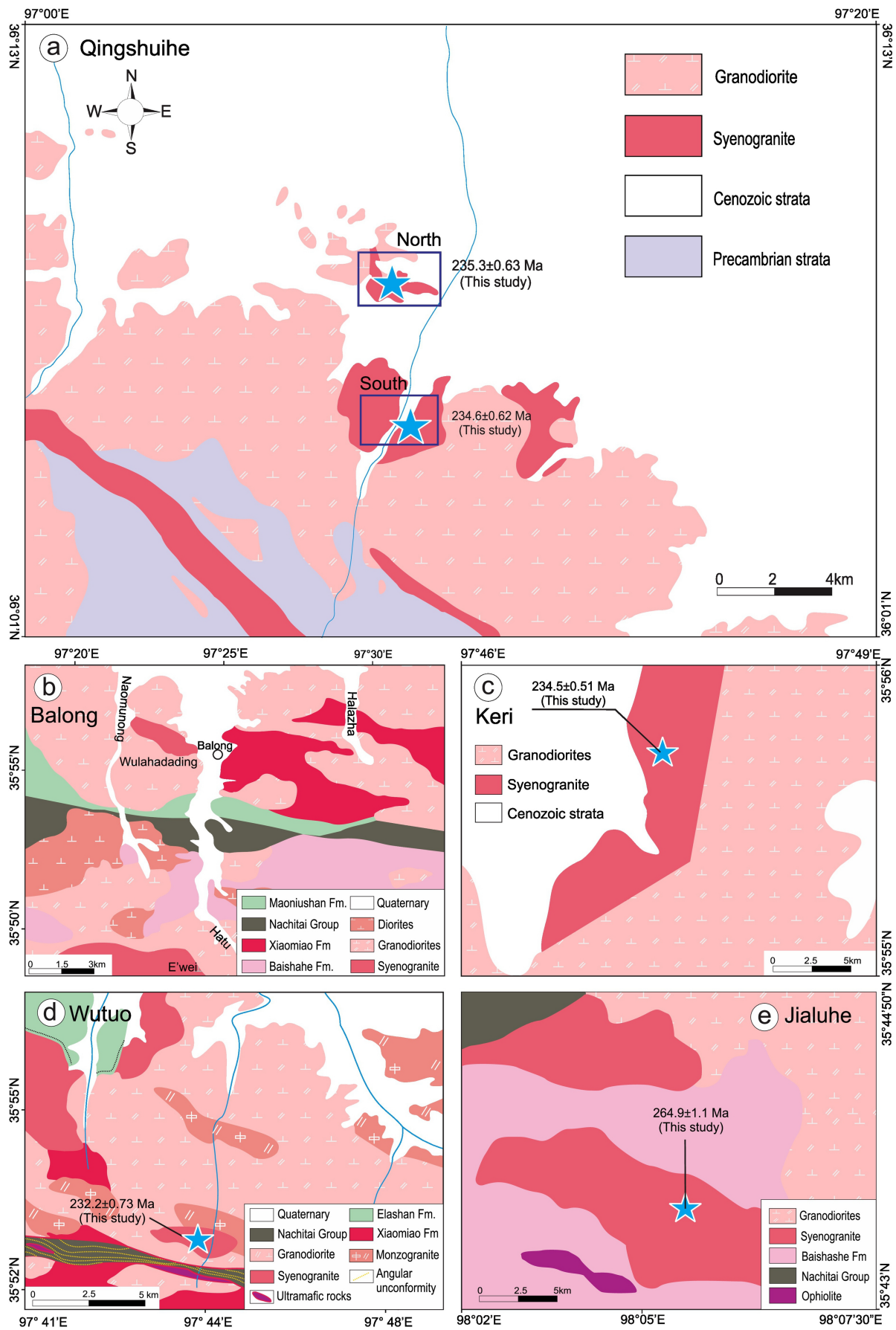


Figure 2

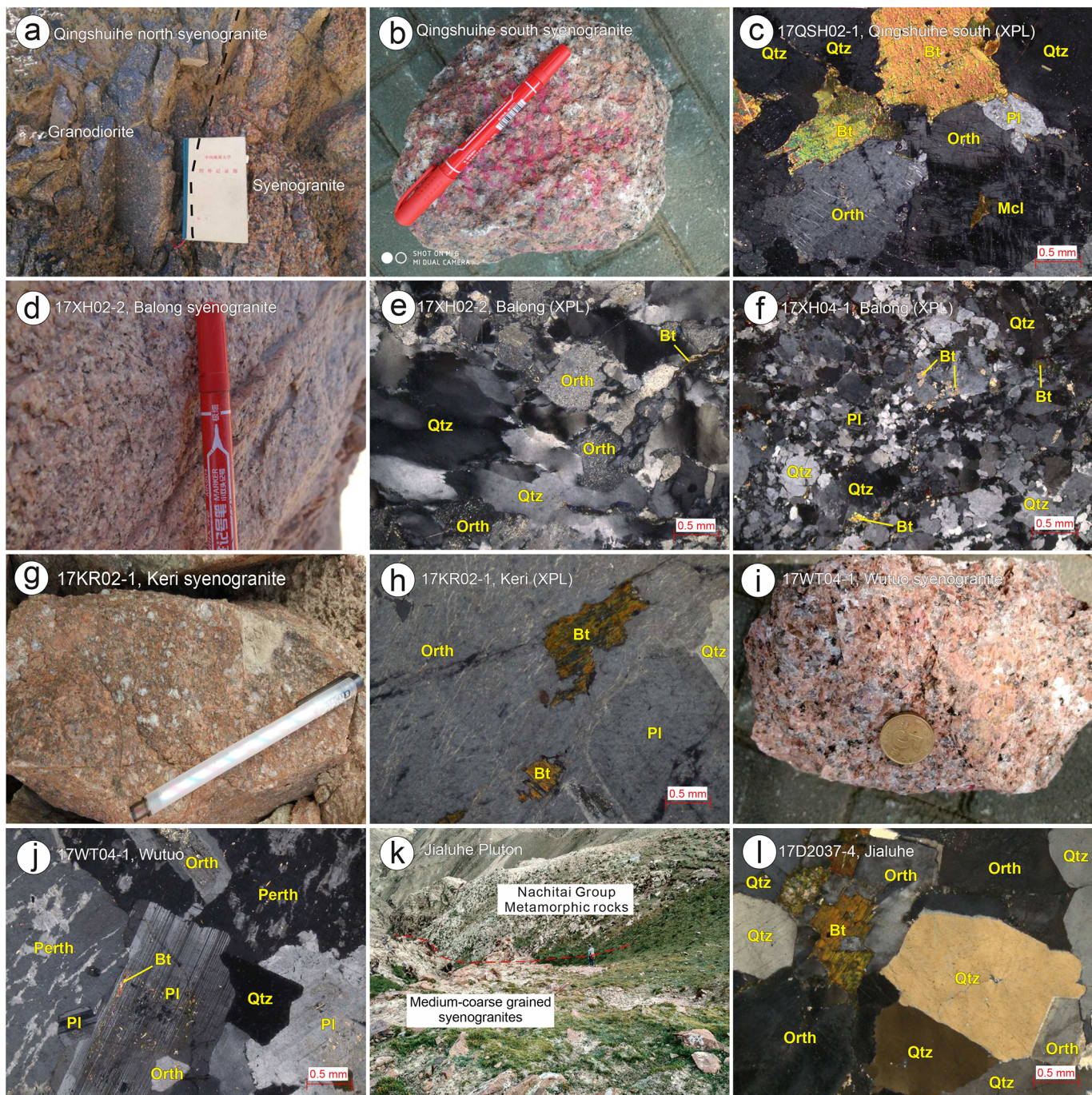


Figure 3

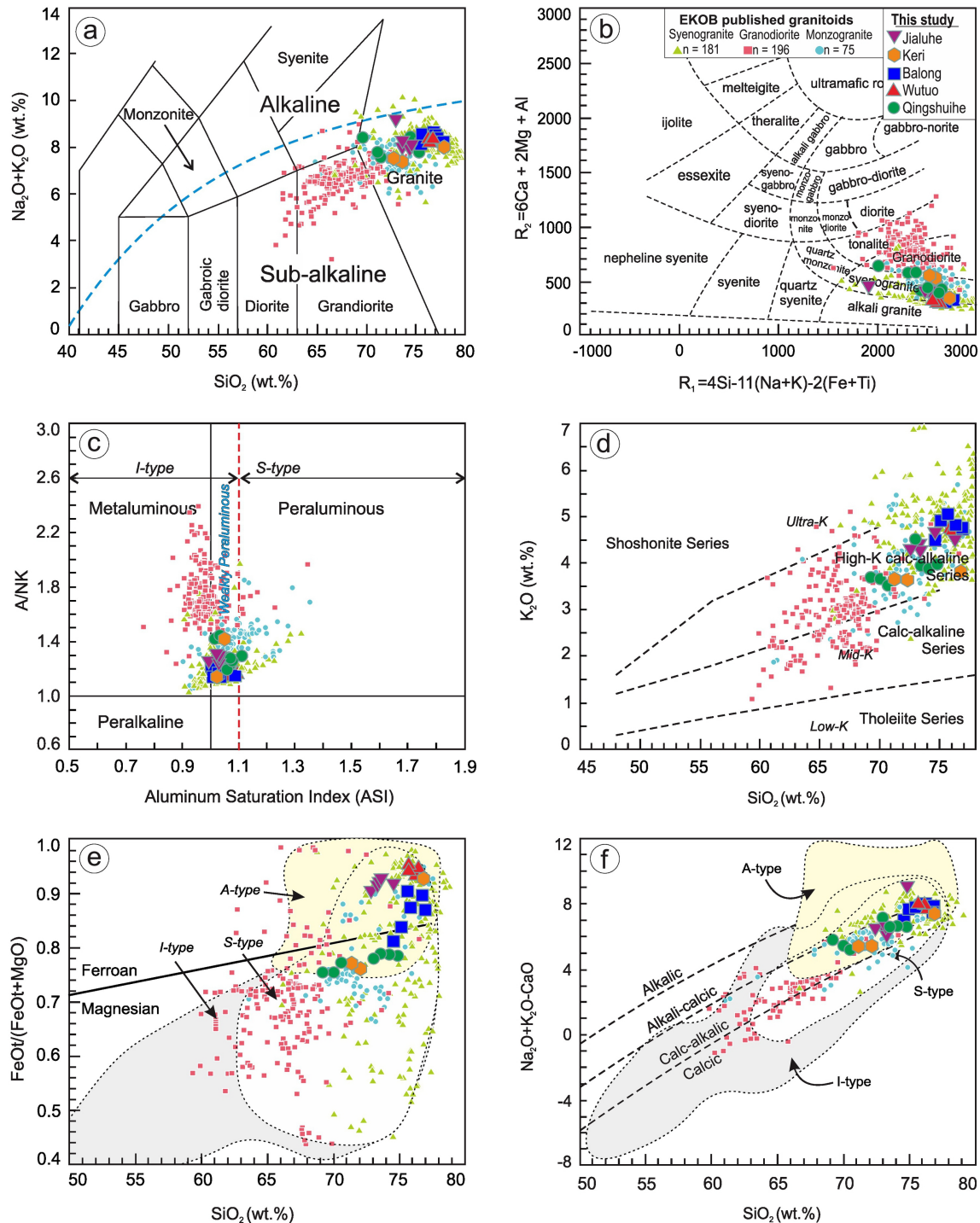


Figure 4

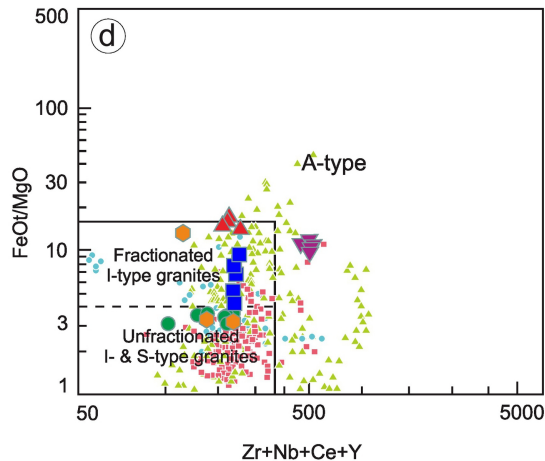
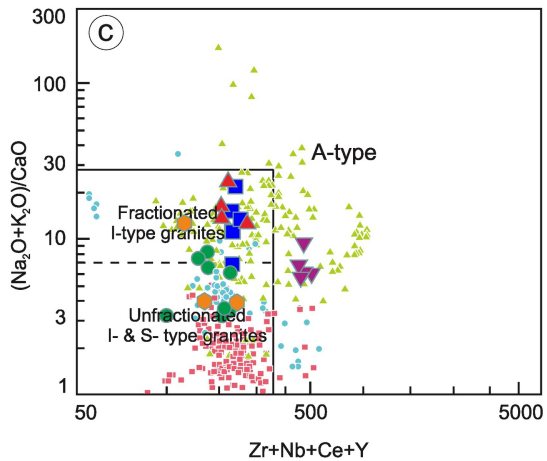
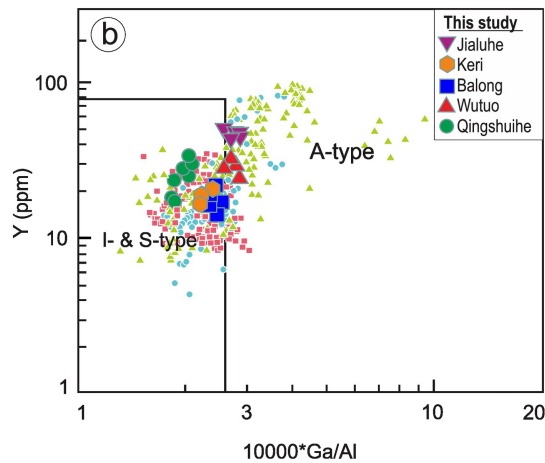
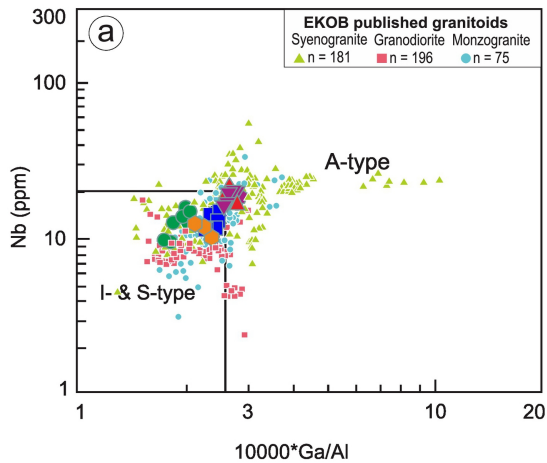


Figure 5

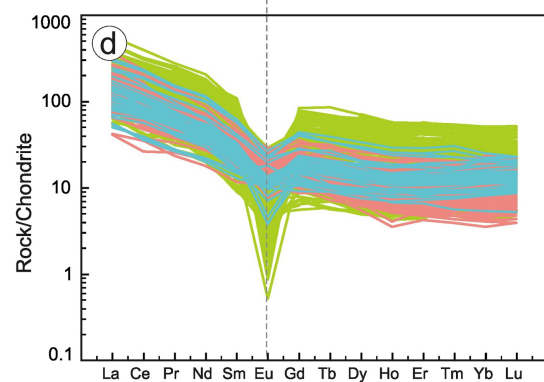
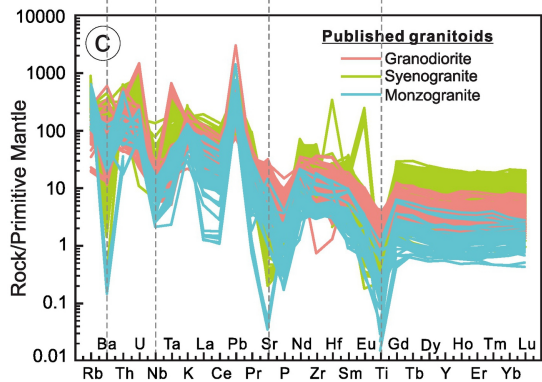
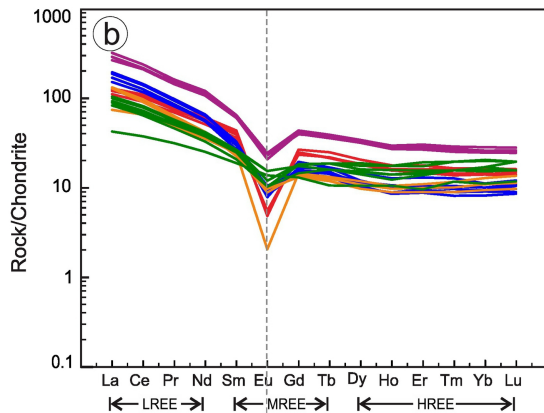
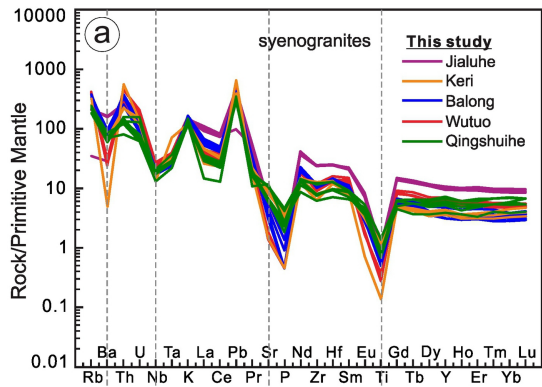


Figure 6

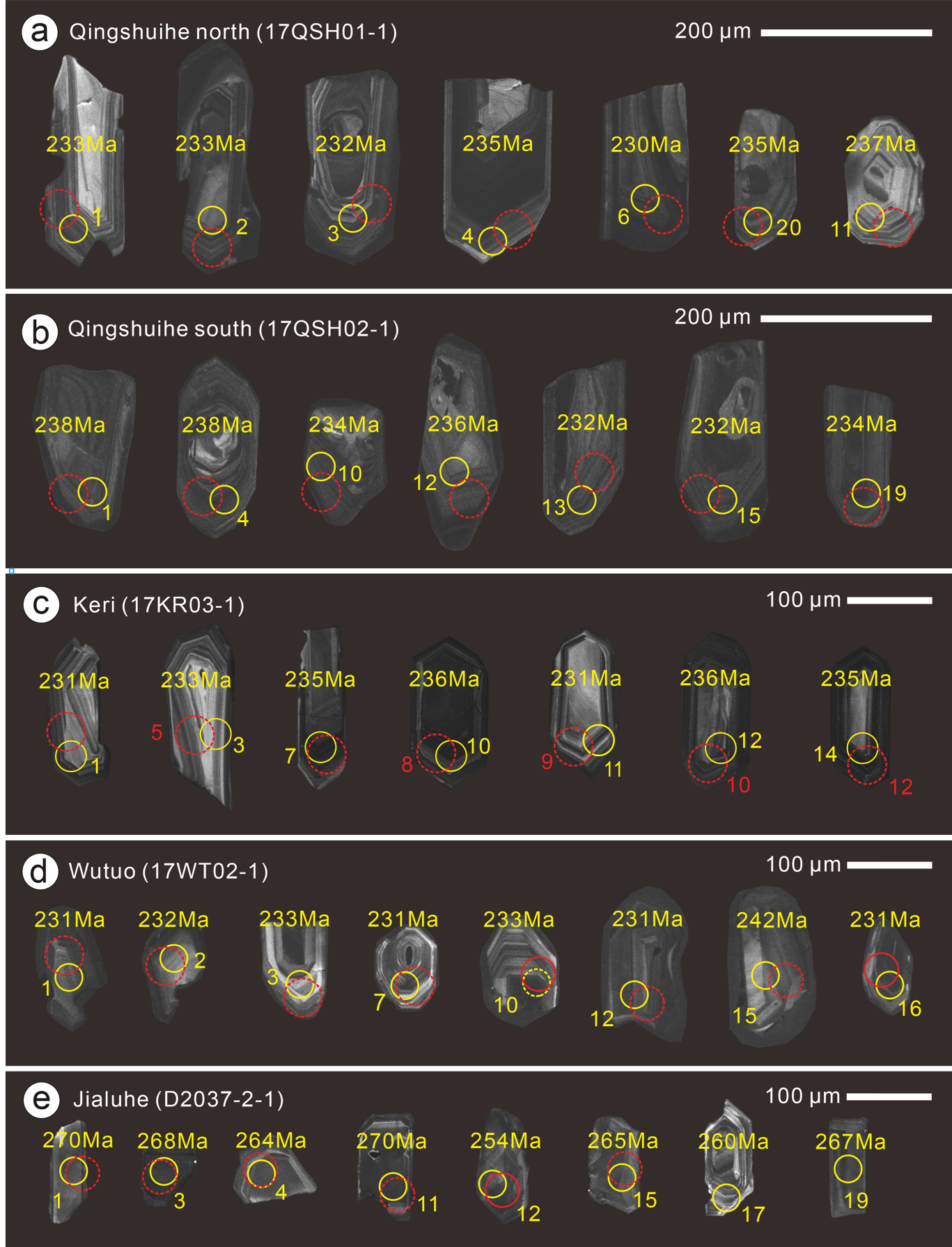


Figure 7

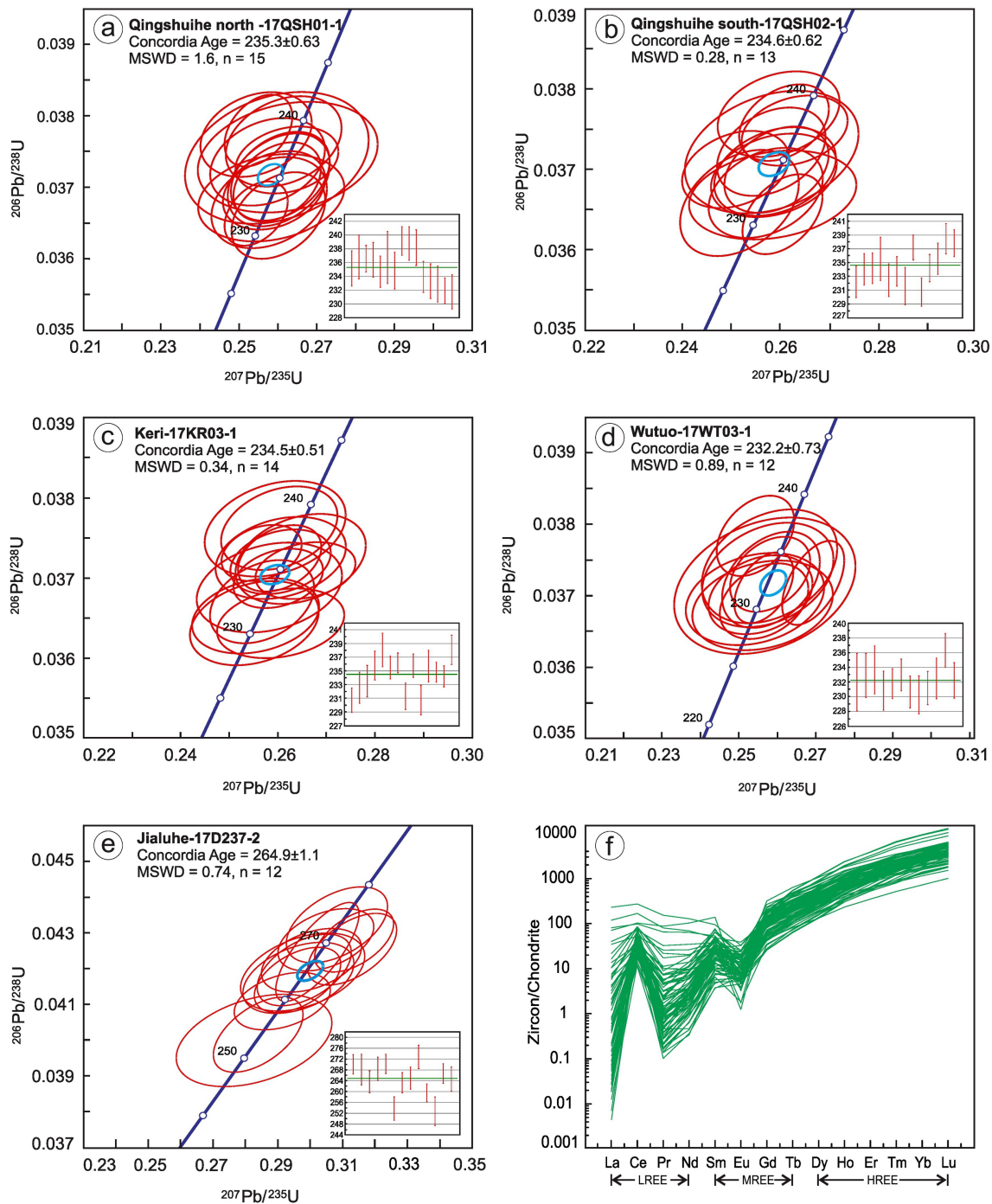


Figure 8

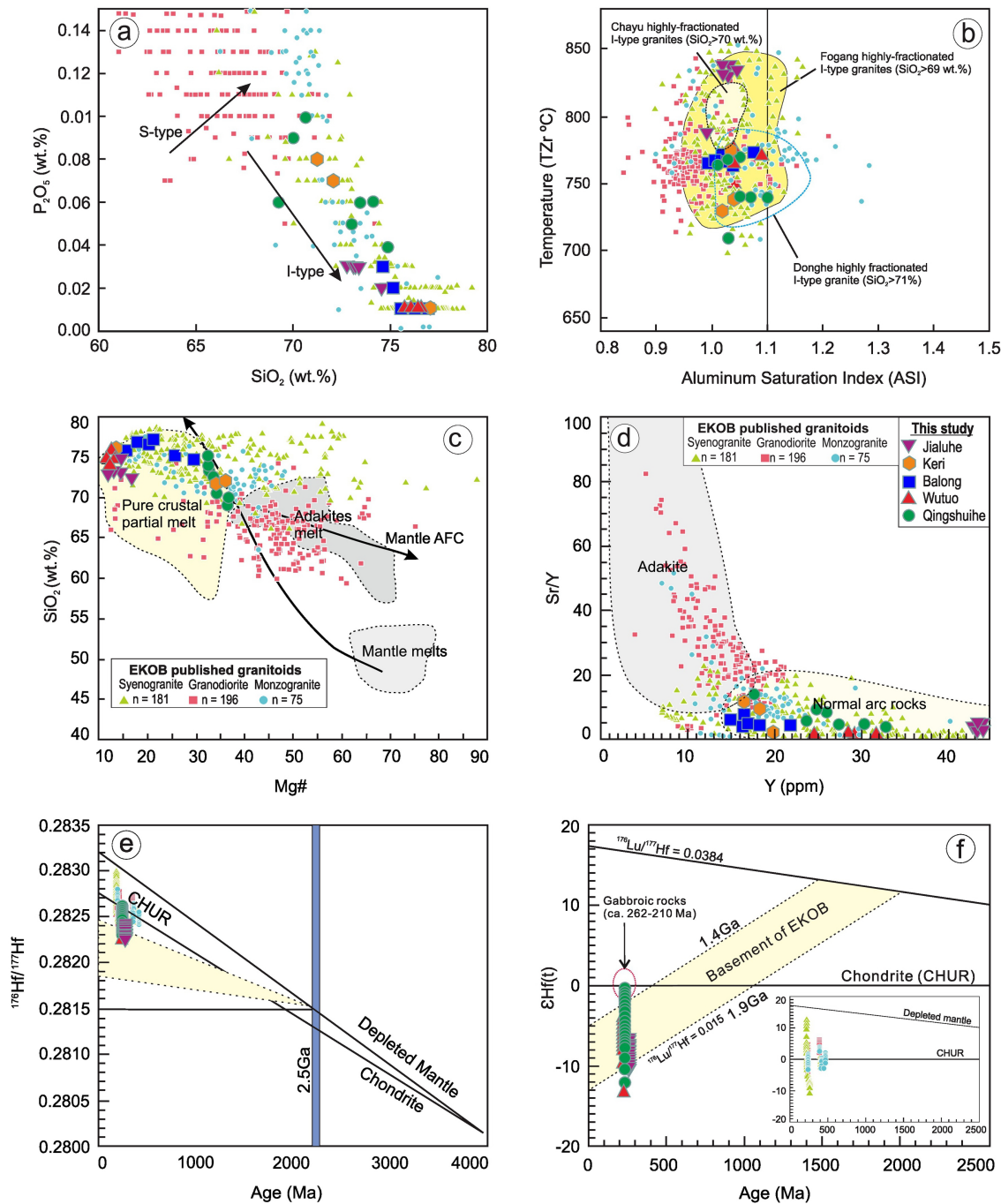


Figure 9

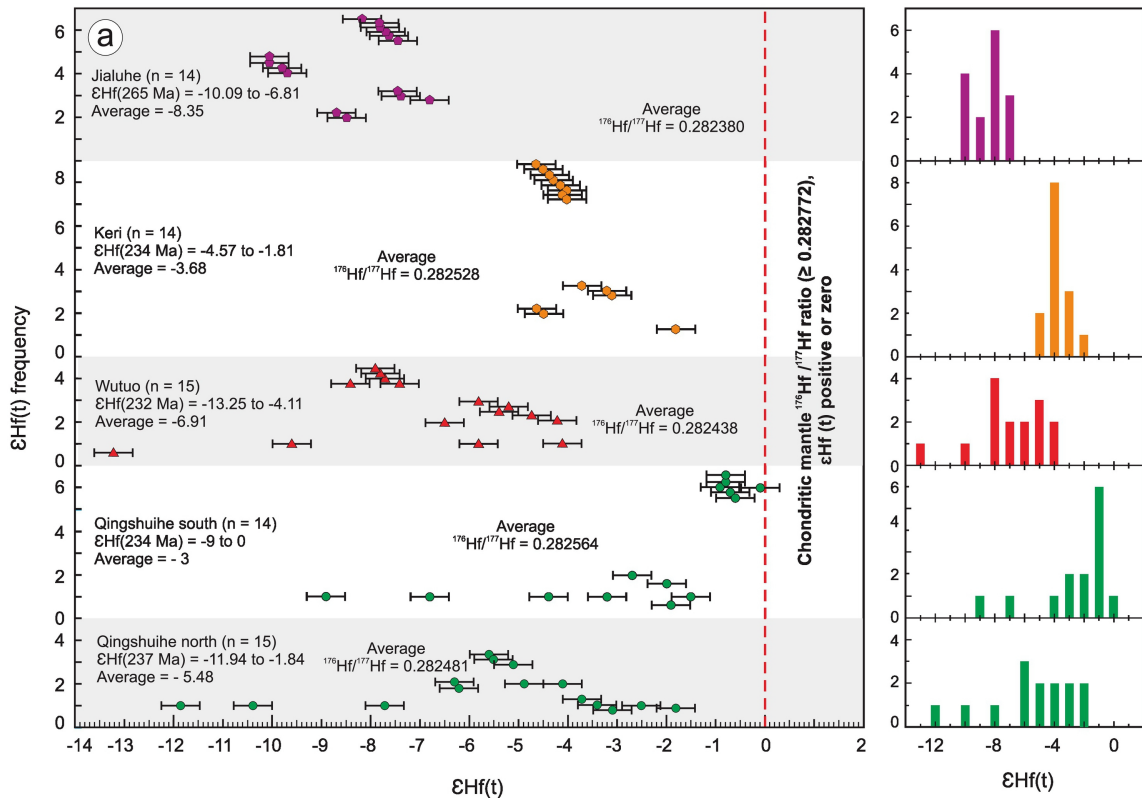


Figure 10

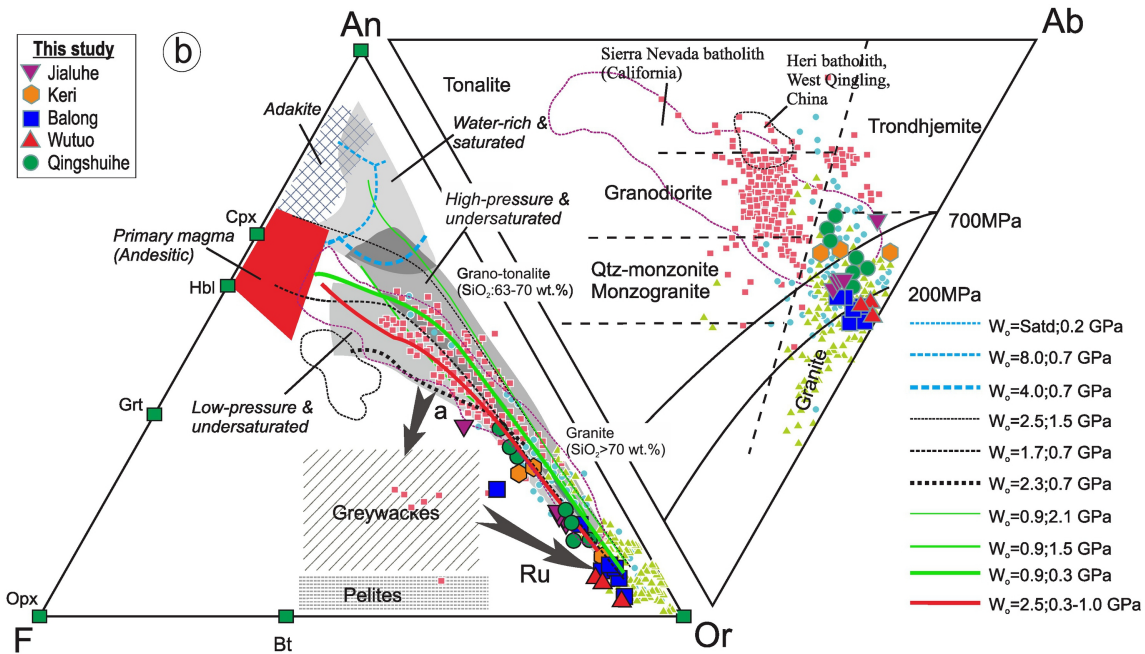


Figure 11

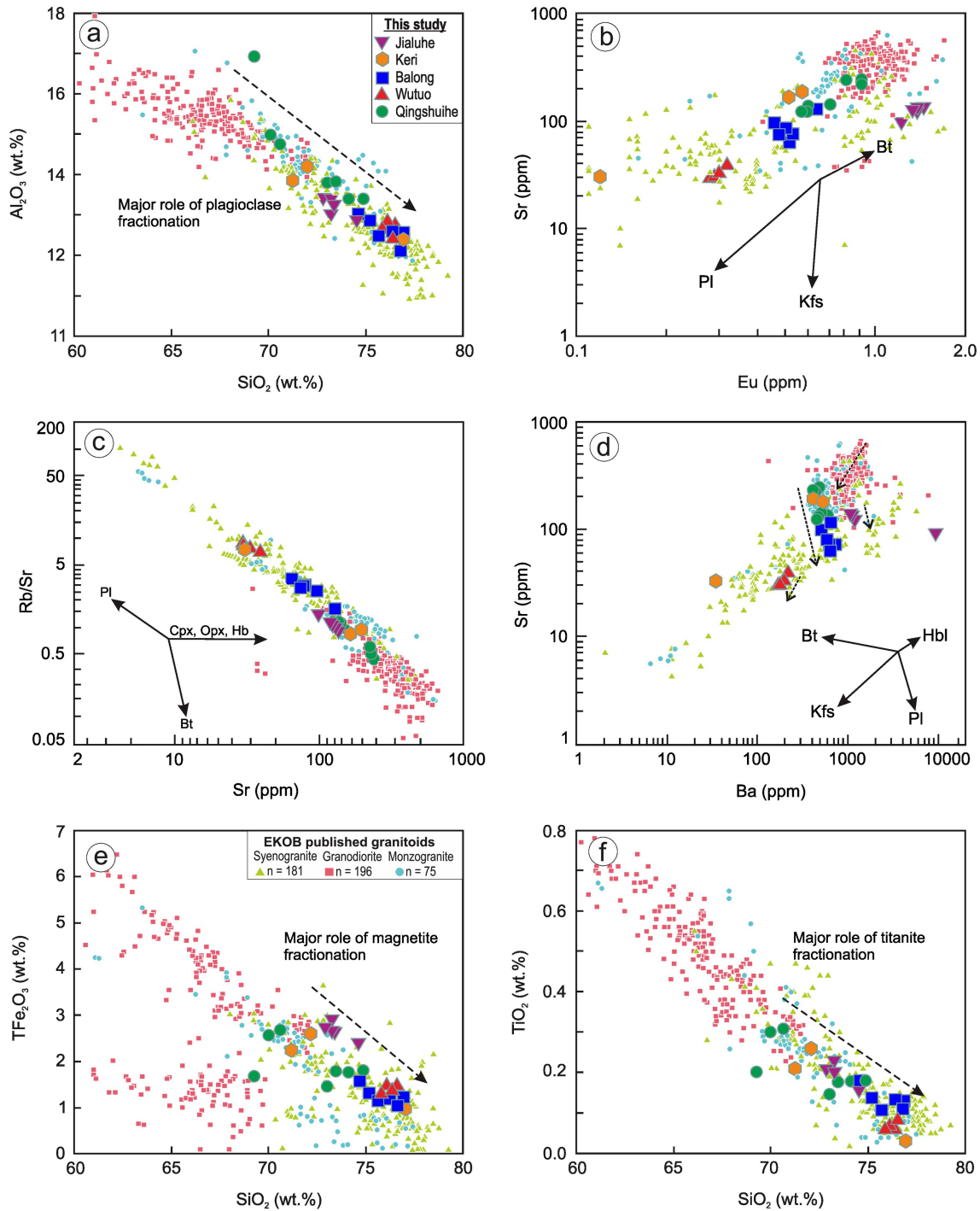


Figure 12

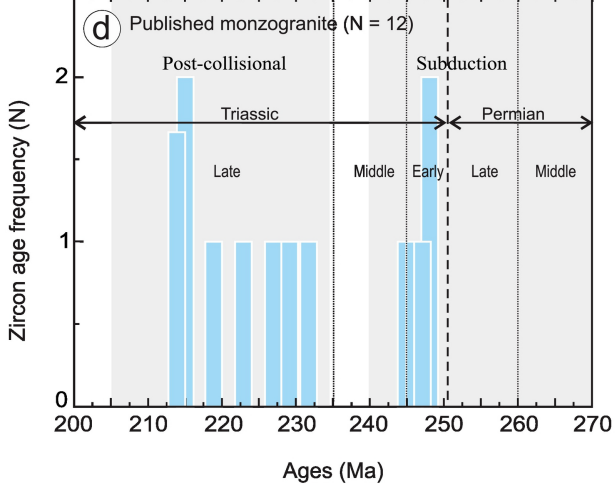
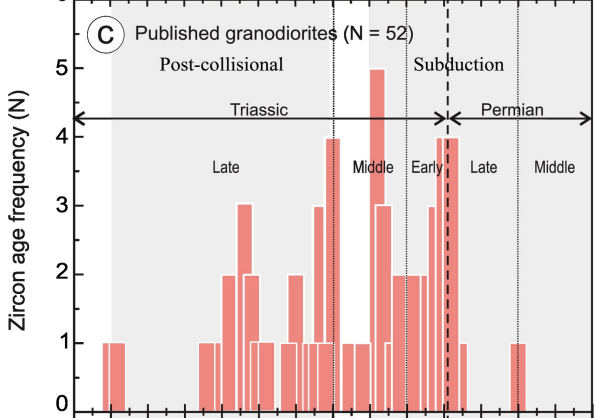
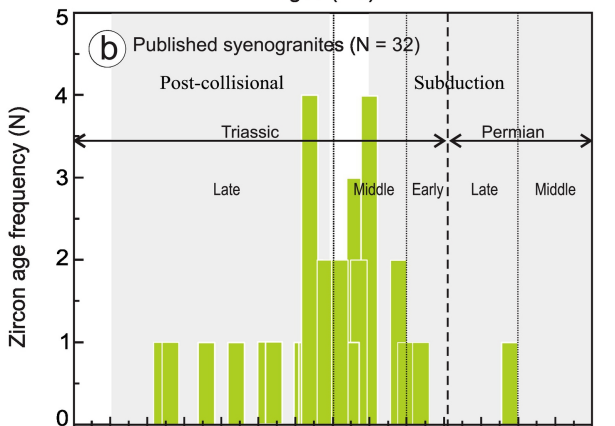
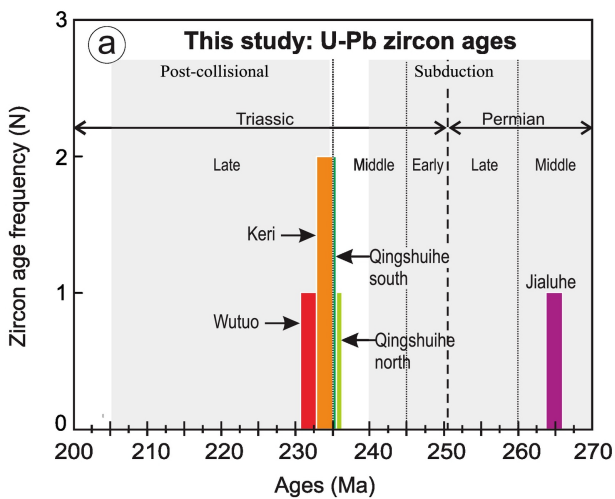


Figure 13

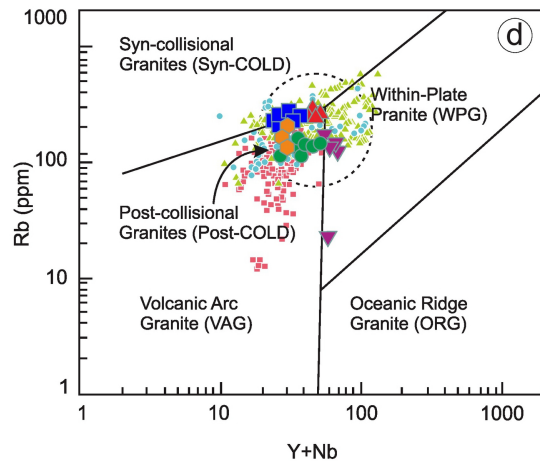
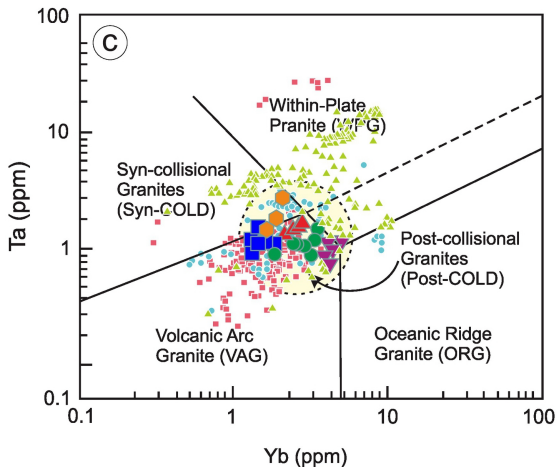
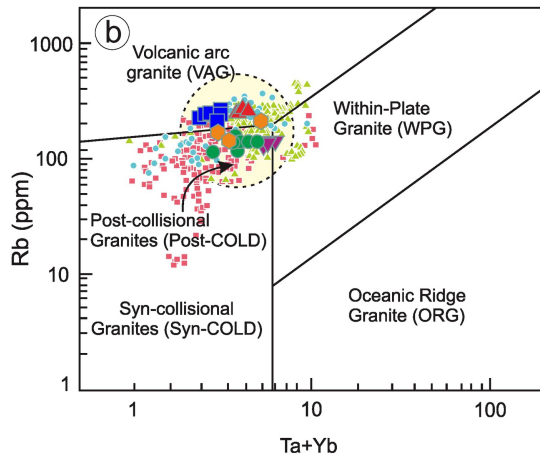
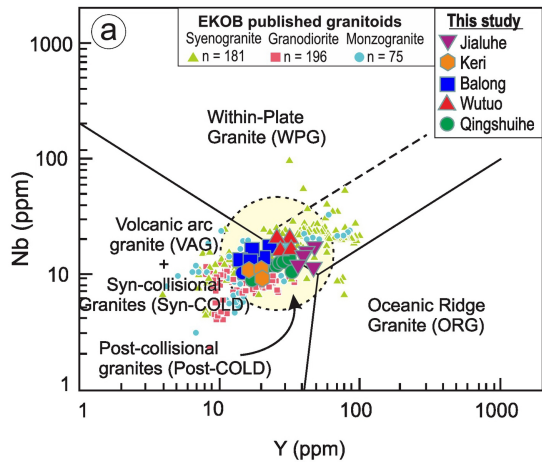


Figure 14

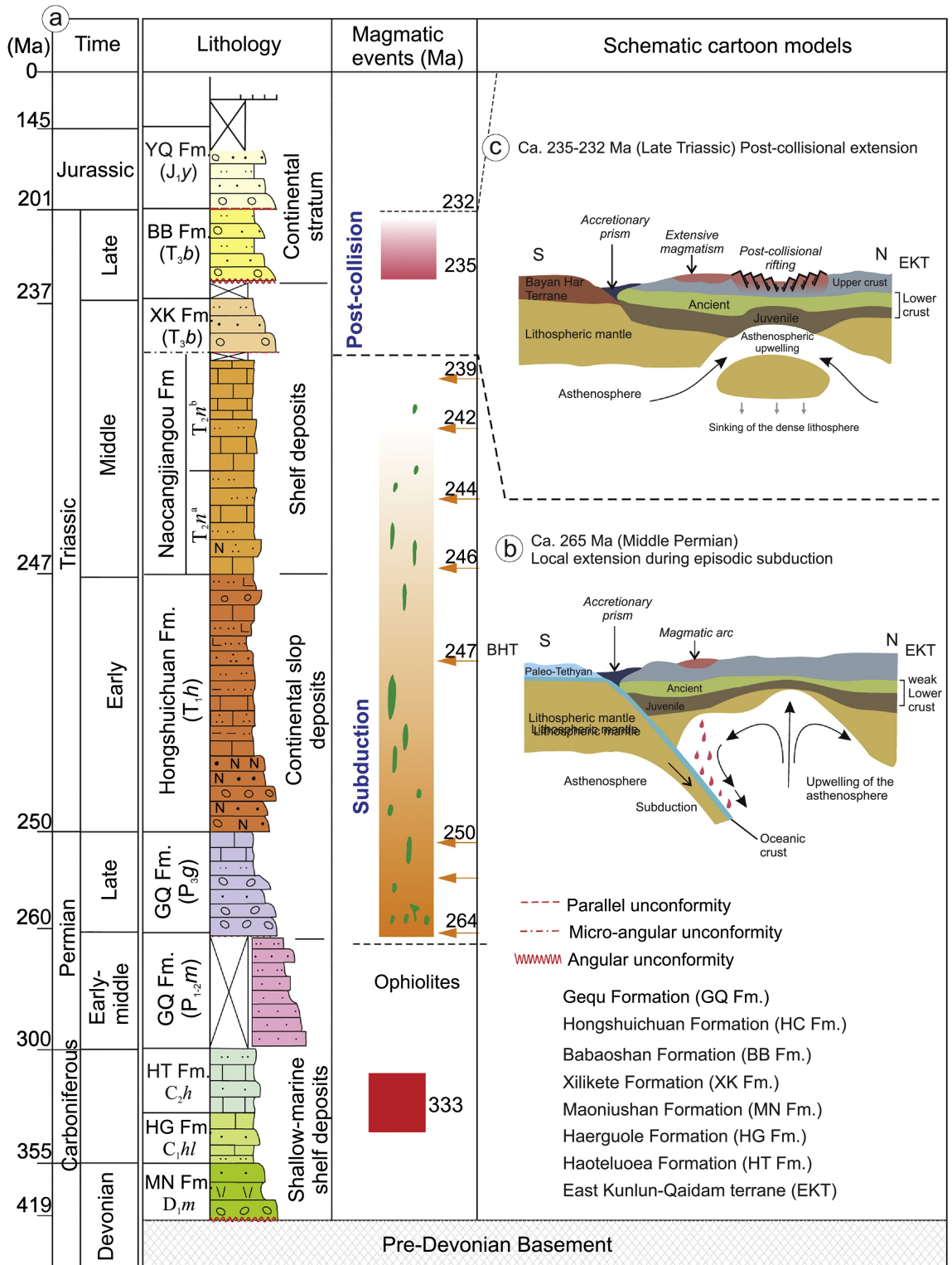


Figure 15